이학박사 학위논문

ENSO 십년주기 변동에 대한 서태평양 표층 바람 응력과 상층 해양 성층화의 역할

Roles of Surface Wind Stress and Upper Ocean Stratification over the Western Pacific on Decadal Changes in El Niño–Southern Oscillation

2013년 8월

서울대학교 대학원

지구환경과학부

이 윤 경

ENSO 십년주기 변동에 대한 서태평양 표층 바람 응력과 상층 해양 성층화의 역할

Roles of Surface Wind Stress and Upper Ocean Stratification over the Western Pacific on Decadal Changes in El Niño–Southern Oscillation

지도교수 허 창 회

이 논문을 이학박사 학위논문으로 제출함
2013년 4월

서울대학교 대학원
지구환경과학부
이 윤 경

이윤경의 이학박사 학위논문을 인준함
2013년 6월

위 원 장 _____ (인)

부위원장 _____ (인)

위 원 _____ (인)

위 원 _____ (인)

위 원 _____ (인)

Dissertation for a Ph.D degree

Roles of Surface Wind Stress and Upper Ocean Stratification over the Western Pacific on Decadal Changes in El Niño–Southern Oscillation

ENSO 십년주기 변동에 대한 서태평양 표층 바람 응력과 상층 해양 성층화의 역할

Yoon-Kyoung Lee

August 2013

School of Earth and Environmental Sciences

The Graduate School

Seoul National University

Roles of Surface Wind Stress and Upper Ocean Stratification over the Western Pacific on Decadal Changes in El Niño–Southern Oscillation

By
Yoon-Kyoung Lee

Dissertation Submitted to the Faculty of the Graduate School of the Seoul National University in Partial Fulfillment of the Requirement for the Degree of Doctor of Philosophy

Degree Awarded:
August 2013

Advisory Committee:

Professor Kwang-Yul Kim, Chair
Professor Chang-Hoi Ho, Advisor
Professor Jong-Ghap Jhun
Professor Soon-Il An
Professor Sang-Wook Yeh

ABSTRACT

Roles of Surface Wind Stress and Upper Ocean Stratification over the Western Pacific on Decadal Changesin El Niño–Southern Oscillation

Yoon-Kyoung Lee
School of Earth and Environmental Sciences
The Graduate School
Seoul National University

El Niño–Southern Oscillation (ENSO) variability is linked to both wind stress variations and recharge/discharge of oceanic heat content in the equatorial Pacific. This dissertation investigates the characteristics of the surface wind stress and the ocean stratification over the western Pacific, and their roles on the decadal changes in ENSO properties. To understand their characteristics, the contribution of the surface momentum forcing to the ocean vertical baroclinic mode is mainly discussed; 1) relationship between the wind stress and ocean stratification, 2) changes in the relationship of oceanic vertical baroclinic mode-ENSO, and 3) recent changes in warm pool SST and its linkage with ocean stratification. The oceanic vertical baroclinic modes associated with ocean stratification, which are derived from the solution of Sturm-Liouville

equation, are investigated to find the effect of wind stress forcing into the ocean. Simple Ocean Data Assimilation (SODA) data (zonal wind stress, ocean temperature, salinity and zonal current) and Hadley sea surface temperature (SST) data were used for the period 1958-2004. In addition, simple coupled model is conducted to understand details of physical mechanism.

In the observation analysis, the wind stress curl over the western Pacific is weakened after the late-1970s than before the late-1970s, which is associated with the slow discharge of heat contents in the equator, leads the long period and strong intensity of ENSO. The simple coupled model experiment verifies that both period and amplitude of ENSO are decreased when the wind stress curl over the western Pacific is projected more strongly into the ocean at the ENSO mature phase.

The wind projection coefficients against the oceanic baroclinic modes have significant change on decadal time scale, in particular, the relationship between the first and second baroclinic modes is reversed before and after the late-1970s. Compared to before the late-1970s, the first baroclinic mode has a greater effect on the sea surface temperature variability through equatorial wave dynamics. It is also found that a delayed-response of the second baroclinic mode variability to the atmospheric forcing has increased after the late-1970s. This reflects the changes in ENSO feedback process associated with the climate shift at the late-

1970s.

The mean SST over the western Pacific warm pool, where the wind stress variation is small, has experienced a shift from cool state to warm state in recent decades. Increased SST enhances the vertical stratification at the upper level. The warm pool SST variability is highly correlated with the change in maximum buoyancy frequency which is captured by the wind stress variations projecting onto the first baroclinic mode over the warm pool region. The zonal wind stress regressed onto the first baroclinic mode before the mid-1970s is associated with the anomalous SST in the eastern and central tropical Pacific. After the mid-1970s, in contrast, a wind convergence pattern near the eastern edge of the warm pool is dominant. The ocean stratification change over the warm pool region, which is related to the changes in wind stress forcing projecting onto the oceanic baroclinic modes, might contribute to change in El Niño structure in the observation during recent decades.

Key words: ENSO, Vertical baroclinic mode, Wind stress, Ocean stratification, Decadal variability, Warm pool

Student Number: 2004-30945

Contents

List of Tables

List of Figures

CHAPTER 1

INTRODUCTION

1.1 Background

It has been observed that the decadal climate shift in the late-1970s accompanies by significant changes in the ocean temperature over the Pacific as well as atmospheric winds (Graham 1994; Guilderson and Schrag 1998; Wu and Xie 2003). After the late-1970s, sea surface temperature (SST) significantly increases over the equatorial central and eastern Pacific with a triangular shape. The structure of ocean interior temperature is also changed with a warming within the subsurface (~30 m) and a cooling around the thermocline depth along the equator (Moon *et al*. 2004; Dewitte *et al*. 2009). In addition, atmospheric trade wind is weakened in the eastern and central tropical Pacific

(Wu and Xie 2003; Vecchi *et al*. 2006). In addition to these changes, El Niño and Southern Oscillation (ENSO) properties including amplitude and frequency have been changed in the recent decades. After the late-1970s climate shift, the period and the intensity of ENSO become longer and stronger. An and Wang (2000) and Wang and An (2001) made an effort to convince the cause of ENSO change with the late-1970s climate shift (Nitta and Yamada 1989; Trenberth and Hurrel 1994; Latif and Barnet 1994; Zhang and Levitus 1997). They suggested that the cause of ENSO change in 1980–90 is due to the change of ocean dynamics with wind forcing change over the tropical Pacific. Also, they showed that the period and intensity of ENSO were increased when the zonal wind stress anomaly was shifted eastward using a simple coupled model.

The variability of ENSO is associated with surface momentum forcing, ocean heat content, and ocean stratification. It has been suggested that the spatial structure of the wind stress forcing in the tropical Pacific can lead to ENSO frequency change (Kirtman 1997; Wang and An 2001). The response of the ocean dynamics to wind stress forcing in the equatorial Pacific is highly dependent on the ocean stratification, which controls the projection of wind forcing onto oceanic baroclinic modes. Since the early work of Lighthill (1969), it is known that momentum forcing input into the ocean can be inferred from the mean stratification within the linear formalism through the so-called projection

coefficient. A physical meaning of the projection coefficient is that the wind stress acting on the ocean depends on its stratification and can be decomposed into input of energy on various vertical mode functions, namely baroclinic modes. To understand ENSO amplitude changes before and after the late-1970s, Moon *et al*. (2004) focused on the variability of the wind stress forcing and their relationship with the equatorial stratification. In particular, in the light of a vertical mode decomposition of the mean stratification before and after the late-1970s, they concluded that the changes of ENSO amplitude are associated with an increased contribution of higher-order modes in the western and central equatorial Pacific.

The western Pacific warm pool region (hereafter, warm pool), where the annual mean SST is consistently higher than 28°C, is closely tied to the surface current variation driven by ENSO-related surface winds (Picaut *et al*. 1996). The variability of warm pool SST is induced from complex interactions between the oceanic and atmospheric mechanism (Clement *et al*. 2005). The warm pool SSTs are capable of modulating deep tropical convections that drive the general circulation in the atmosphere and thus allow influence global heat, water, and energy cycles (Fu *et al*. 1994; Ramanathan et al. 1995; Pierrehumbert 1995; Visser *et al*. 2003; Clement *et al*. 2005; De Garidel-Thoron *et al*. 2005; Wang and Mehta 2008). Recent studies have suggested that the warm pool SST is increasing over

the last century in a similar fashion to the global mean surface air temperature (Sun 2003; Wang and Mehta 2008; DiNezio *et al*. 2009). Increase of the warm pool SST can change surface winds, which in turn change ocean currents connecting the western tropical Pacific Ocean with the eastern tropical Pacific Ocean (Sun and Liu 1996). These changes are ultimately associated with the SST variability such as ENSO. In addition, changes in the warm pool SST on the low frequency timescales may determine the tropical Pacific mean state toward "El Niño-like" or "La Niña-like" mean state (Vecchi and Soden 2007; DiNezio *et al*. 2009, 2010) which has an impact on ENSO properties such as amplitude and frequency by changing thermocline feedback processes and zonal advective feedback processes (Nitta and Yamada 1989; Picaut *et al*. 1996; Knutson *et al*. 1997; Cane *et al*. 1997; Fedorov and Philander 2000; Sun 1997; 2003; Luo *et al*. 2003; Collins *et al*. 2005; 2010; Kim and An 2011, An *et al*. 2012). These previous studies suggest that the changes in the warm pool SST are able to influence the tropical Pacific SST variability through different physical processes.

There is another way by which changes in the warm pool SST may alter the atmosphere-ocean coupled system in the tropical Pacific, which has not been much investigated so far. That is, changes of warm pool SST induce changes in the vertical temperature structure by modifying the vertical temperature gradient in the vicinity of the thermocline and thereby constraining the energy

distributed over oceanic vertical baroclinic modes in the warm pool region. According to previous studies, small changes in the mean vertical temperature for the 0–500 m depth are projected onto the gravest baroclinic modes which lead to the associated fluctuation in the equatorial wave characteristics (Dewitte *et al*. 2009) and ultimately result in the change of ENSO properties (Dewitte 2000; Dewitte *et al*. 2007; Moon *et al*. 2004, 2007).

Interestingly, recent studies have suggested that there are two different types of El Niño: conventional El Niño and non- conventional El Niño. While the conventional El Niño typically exhibits SST variations in the cold tongue region of the eastern equatorial Pacific, the non-conventional type of El Niño is characterized by maximum SST variations in the central equatorial Pacific (Larkin and Harrison 2005a, 2005b; Ashok *et al*. 2007; Kao and Yu 2009; Kug *et al*. 2009). Furthermore, non-conventional El Niño has occurred more frequently during recent decades (Ashok *et al*. 2007; Yeh *et al*. 2009; Lee and McPhaden 2010). Yeh *et al*. (2009) showed that using the Coupled Model Intercomparison Project phase 3 (CMIP3) multi-model dataset, the tendency toward more occurrence of the non-conventional El Niño (i.e., Modoki El Niño) in a warmer climate may be related to the increased stratification in the vicinity of the thermocline although there are some debates on this issue (McPhaden *et al*. 2011).

1.2 Motivation and Objective

Investigating the change in the wind projection coefficient through the change in stratification can thus bring insights for interpreting the interannual SST variability in the equatorial Pacific (i.e., ENSO). Until now, there have been a few investigations to analyze on the variability of the wind projection coefficient after the late-1970s climate shift in the equatorial Pacific. Most of studies only focused on the change on a decadal time scales in ENSO (Moon *et al*. 2004; Dewitte *et al*. 2007). In the present dissertation, the author highlights the importance of these changes on a decadal time scale, relationship change in decadal time scale for interpreting the ENSO feedback processes, and ENSO properties. Due to the coupled nature of ENSO, the actual underlying processes associated with the change in wind stress forcing remains unclear. A better description of these changes and their relation to the ENSO variability are needed. The author clarify how the wind stress variation and ocean stratification over the western Pacific can affect the ENSO change which occurred after the climate shift.

There is an observational evidence that the warm pool SST exhibits a positive trend over the last decades (Cravatte *et al*. 2009; Kim and An 2011), which would tend to enhance the vertical temperature gradient between the surface

layer and the thermocline depth temperature. Therefore, this raises a question to which extent the warm pool SST change reflects the change in stratification that is influential on the tropical Pacific SST variability. This question motivates the present dissertation that focuses on the relationship between the tropical Pacific SST variability and the changes of the vertical temperature structure in the warm pool region.

The issue on the source of the ENSO modulation in the tropical Pacific has drawn the considerable interest in recent years. Indeed, it has not been clear to what extent the change in ENSO characteristics on decadal time scale is due to external forcing from the atmosphere through teleconnections (Pierce *et al*. 2000) or from ocean through the oceanic tunnels (Gu and Philander 1997; Luo and Yamagata 2001; Giese *et al*. 2002; Luo *et al*. 2003; Moon *et al*. 2007). Also, it is not clear that the ENSO equatorial dynamics can produce its own decadal variability through nonlinearities (Timmermann and Jin 2002; Timmermann 2003; Rodgers *et al*. 2004; Yeh and Kirtman 2004; Dewitte *et al*. 2007).

Changes in the wind stress forcing projecting onto the first baroclinic mode in the warm pool region, which are related to changes in vertical stratification, may thus contribute to the change of ENSO structure. It is a very important task to understand how the ENSO has been changed under the recent climate variability. To understand characteristics of ENSO change which will be

appeared in the future, several studies about the role of tropical mean field change have been reviewed (Timmermann *et al*. 1999; Collins 2000; Guilyardi 2006). But exact understanding about relationship between the mean field change and ENSO is not sufficient, so far. Due to the coupled nature of ENSO, the actual underlying processes associated with the change in wind stress forcing remain unclear. A better description of these changes and their relation to the ENSO variability is needed.

A study on the effect of the wind stress and ocean stratification to the ENSO variability is important. ENSO variability is linked to wind stress and recharge/discharge of oceanic heat content associated with the thermocline depth in the equatorial Pacific. The objective of this dissertation is to find the characteristics of wind stress and ocean stratification and their roles in the ENSO decadal changes.

This dissertation is organized as follows.

Chapter 2 describes the data and methods to decompose of ocean vertical baroclinic modes and projection coefficients on the each mode. In chapter 3, the characteristics of wind stress with ocean heat content, its impact on ENSO properties, and decadal changes in ENSO properties are investigated. Chapter 4 shows the decomposition of vertical baroclinic mode, and their contribution to ENSO evolution and spatial structure. And recent decadal changes in warm

pool SST and its linkage with ocean stratification are also described. The results of this dissertation are summarized in chapter 5.

CHAPTER 2

DATA AND METHODS

2.1 Data

2.1.1 Simple Ocean Data Assimilation (SODA)

The SODA reanalysis project, which began in the mid-1990s, is to reconstruct historical ocean climate variability on space and time scales similar to those captured by the atmospheric reanalysis projects.

SODA data which is based on Modular Ocean Model version 2 (MOM2) of Geophysical Fluid Dynamics Laboratory were used in this dissertation. The horizontal resolution is 0.5°×0.5° and 40 levels in the vertical with 10-m spacing near the surface. The data used in this dissertation are the monthly sea surface temperature, salinity, wind stress, current which are derived from SODA

version 2.0.2 (from January 1958 to December 2001) and version 2.0.3 (from January 2002 to November 2005). The SODA system is useful to examine the oceanic variables in the subsurface layers and shows the characteristic changes of mean state in the ocean before and after the late-1970s (Moon *et al*. 2004; Dewitte *et al*. 2009). Therefore, it is appropriate to conduct the vertical mode decomposition using the temperature and salinity data in the SODA system. The constraint algorithm is based on optimal interpolation data assimilation. Assimilated data includes temperature and salinity profiles from the World Ocean Atlas 2001 [mechanical bathythermograph (MBT), XBT, CTD, and station data (Conkright *et al*. 2002), as well as additional hydrography, SST, and altimeter sea level. The model was forced by daily surface winds provided by the 40-yr European Centre for Medium-Range Weather Forecasts (ECMWF) Re-Analysis (ERA-40; Uppala *et al*. 2005) for the 48-yr period from January 1958 to November 2005. The reader is invited to refer to Carton *et al*. (2000) and Carton and Giese (2008) for a detailed description of the SODA system.

2.1.2 Hadley Centre Sea Surface Temperature

The SST analysed in this study is taken from the Hadley Centre SST dataset (HadISST, Rayner *et al*. 2003) for the period 1958–2004. The HadISST is based on

the data contained within the recently created Comprehensive Ocean and Atmosphere Data Set (Woodruff *et al*. 1998) with a relatively high spatial resolution of 1° by 1° and it is superior in geographical coverage to previous datasets and has smaller uncertainties (Rayner *et al*. 2003). The starting year of the HadISST dataset is 1870, however, analysis period is limited from 1958 to 2004.

The boreal winter season in section 4.2 and 4.3 was focused, which is the typical peak season for ENSO variability. The boreal winter as the five months from October to February for the SST data and atmospheric variables was defined. For example, the 1958 winter thus indicates from October (1958) to February (1959). Unless stated otherwise in the text, the results are for the winter season only. Note that seasonal means are calculated from the monthly data during winter and seasonal anomalies are obtained by subtracting seasonal means from the total (1958–2004) winter mean field.

2.2 Methods

2.2.1 Vertical mode decomposition

The horizontal scale is much larger than the vertical scale in the ocean. Thus, the variables of oceanic motion can be presented as the summation of the normal mode. These variables are expressed as vertical modes as follows (Cane 1984), where the barotropic mode (n=0) was excepted.

$$u(x,y,z,t), v(x,y,z,t), \rho^{-1}p(x,y,z,t) = \sum_{n=1}^{\infty} [u_n{}'(x,y,t), v_n{}'(x,y,t), gh_n{}'(x,y,t)]\, A_n(z)$$

The vertical structure function, $A_n(z)$ (Fig. 2.1) is the solution of eigenvalue-eigenfunction problem (i.e., Sturm-Liouville problem) consists of Brunt-Väisällä frequency number $N(z) = \sqrt{-g\rho^{-1}\partial_z\rho}$. That is, $A_n(z) = \partial_z G_z(z)$ and $\partial_{zz}G_n(z) + \frac{N^2(z)}{{c_n}^2} G_n(z) = 0$

Where, c_n is the propagating speed and $G_n(z)$ is the function which represents the vertical baroclinc mode against to vertical velocity. It was considered that the boundary condition is the zero vertical velocity at the sea surface and the bottom, and $A_n(z)$ is obtained by using the method suggested by Pryce (1993).

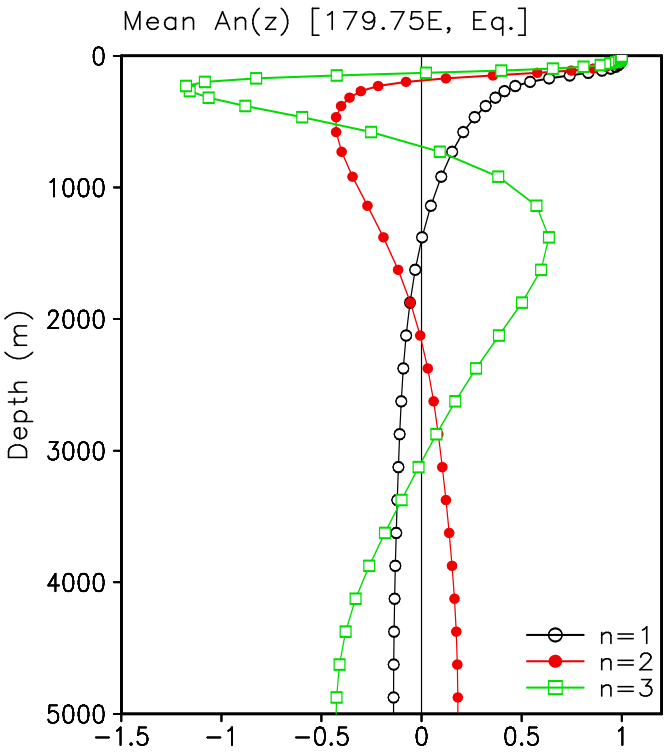

Fig. 2.1. The mean vertical structure functions $A_n(z)$ (n=1, 2, 3) from the surface to 5000 m ocean depth at [179.75°E, Eq.] during 1958-97. See the text for a detailed definition of $A_n(z)$.

2.2.2 Projection coefficient

The projection coefficient of the wind stress onto the baroclinic modes can be inferred and written as follows $P_n = \frac{\int_{-H_{mix}}^{0} A_n(z)dz}{\int_{-H_{mix}}^{0} {A_n}^2(z)dz}$, where H_{mix} is the mixed layer depth and D is the depth of the ocean bottom (cf. Lighthill 1969). Assuming that the gravest vertical modes do not vary much within the mixed layer and using a normalization coefficient of 150 (corresponding to the mean thermocline depth in the central equatorial Pacific), the wind projection coefficient becomes:

$$P_n = \frac{150}{\int_{-D}^{0} {A_n}^2(z)dz} \text{ (n = 1,2,3)}$$

Where, P_n is indicative of surface momentum flux projecting onto the baroclinic modes. It is calculated here from the SODA stratification on each grid point and time step following a similar methodology than in Dewitte *et al.* (1999).

Note that the author hypothesize that changes in wind projection coefficient reflect the actual variability of the baroclinic modes. It was checked that the first Empirical Orthogonal Function (EOF) of $h_n(x, y, t)$ is highly correlated with $P_n(t)$. The correlation coefficients between $P_n(t)$ for the first three baroclinc modes and the first principal component time series of the $h_n(x, y, t)$ over the

region [120°E–280°E, 10°S–10°N], reach 0.52, 0.62, and 0.61, respectively. $h_n(x,y,t)$ is calculated by projecting the pressure anomaly field onto the mean vertical structure functions, i.e., $gh_n(x,y,t) = \int_{-D}^{0} \overline{A_n}(x,y,z) \cdot \tilde{p}(x,y,z,t)dz$, where $\overline{A_n}$ is the vertical mode structure functions associated with the mean stratification and $\tilde{p}$ is the pressure anomaly field. The advantage of using the $P_n(t)$ instead of $h_n(x,y,t)$ for diagnosing the vertical structure variability is twofold. First, it is much more computational cost effective and second, it can be more easily interpreted in terms of momentum forcing onto the ocean dynamics. In particular, $h_n(x,y,z,t)$ is a complex combination of free and forced equatorial waves and its interpretation in terms of its impact on ENSO feedbacks is difficult due to the non-linear nature of the mixed-layer processes with regards to the baroclinic modes.

The statistical significant test used in this study is basically based on a t-test and the effective degree of freedom to calculate the statistical significance is obtained by the methodology in Livezey and Chen (1983).

CHAPTER 3

WIND STRESS VARIATION AND ENSO

3.1 Wind stress associated with ocean heat content

Surface wind stress change is associated ocean heat contents. The singular value decomposition (SVD) analysis for the zonal wind stress and thermocline depth was carried out to examine the wind stress variation over the western Pacific which is associated with the change of the ENSO (Fig. 3.1). The first SVD mode explains about 51.7 % of total variance and the second SVD mode does about 18.1 % of that, respectively. The first SVD mode represents the quasi-equilibrium state between the pressure gradient force and zonal wind stress, which is called Sverdrup balance. The pressure gradient force is generated by the zonal difference of thermocline depth (Jin 1996). Fig. 3.1a and b show that there are positive (negative) anomalies of the thermocline depth in the eastern

(western) Pacific when the wind stress acts on east-direction. It stands for the state of the mature or peak of the warm phase of ENSO (El Niño). The signals of the zonal wind stress and thermocline depth turn into the opposite sign in the cold phase of ENSO (La Niña). The location of center of the second mode for zonal wind stress is shifted to the west comparing to the first mode. The distribution of the thermocline depth is in contrast to meridional direction. That is, thermocline depth has positive anomalies in the equator and negative anomalies in the sub-tropics, respectively. The zonally positive anomalies of the thermocline depth are distributed around ±5° centered on the equator. The meridional contrast is more evident in the Northern Hemisphere than in the Southern Hemisphere. The zonal-mean thermocline depth changes from negative phase to positive phase with ENSO progress.

The zonal-mean thermocline depth anomalies are not in equilibrium with the zonal wind stress differently from in the case of the zonal thermocline depth. Non-equilibrium between zonal-mean thermocline depth anomalies and wind stress occur the change of ENSO phase as a potential role of air-sea system. This is because that the ocean is slowly adjusted to the wind stress. Jin (1997) suggested that the shallowing of the thermocline depth during the positive phase of ENSO gives rise to the negative phase (recharge oscillator). The decrease of the thermocline depth at the equator means the discharge of the

ocean heat content. The heat content is recharged through the mass convergence from the sub-tropics to equator, which induces ENSO transition from negative phase to positive phase.

The second SVD mode indicates the transition phase of ENSO period (Wang *et al*., 1999). Fig. 3.2 shows results of band-pass filter of time-coefficients by SVD analysis. The period is 2-6 year and there is a little phase difference between the first and the second mode of the time-coefficients. It is noteworthy that the second mode leads the first mode. Kang and An (1998) refer this difference is about 90° by simple model result.

When the heat content is maximum in the tropical Pacific, the wind stress over the western North Pacific is cyclonic circulation. After the 90° phase, the heat content in the equator is discharged to sub-tropics. The change of wind in the western North Pacific and heat content in the equator is explained as following mechanism (An and Kang 2001; Wang *et al*. 1999). The cyclonic circulation might decrease the thermocline depth in this region through acting of Ekman pumping. Decreased thermocline depth propagates westward by Rossby wave and then reflects at the western boundary in the tropical ocean. The reflected Rossby wave turns into Kelvin wave near the equator, and propagates eastward. The Kelvin wave with the decreased thermocline depth reduces the heat content at the equator propagates eastward because the

thermocline depth generated by Ekman pumping is not changed. Similarly, the anticyclonic circulations will play a role for the accumulation of the heat content in the equatorial Pacific. Therefore, the change of the wind stress over the western North Pacific that exists in the second mode affects the redistribution of the heat content and finally induces the ENSO characteristics change.

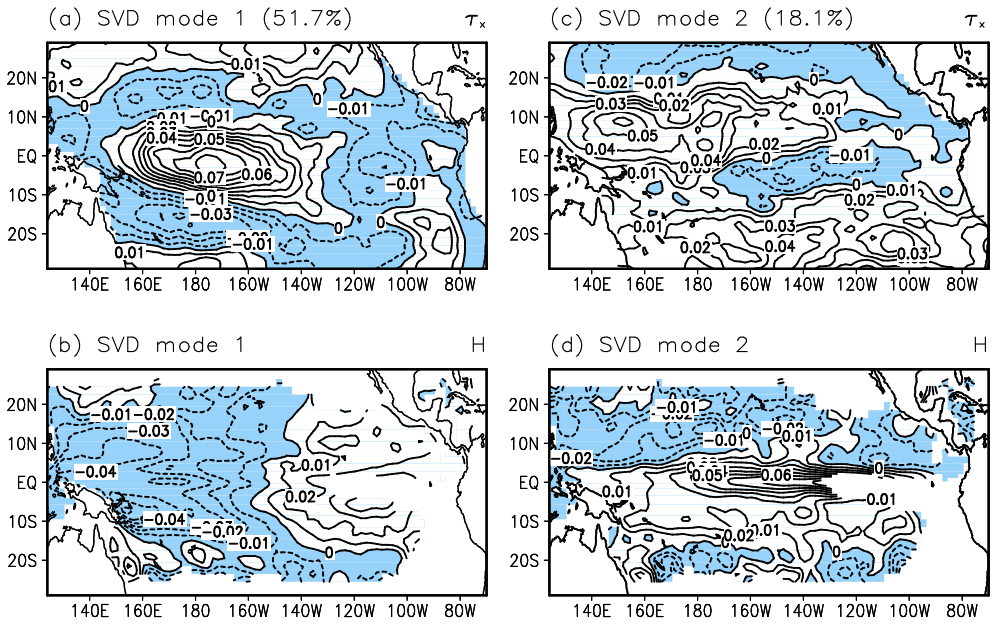

Fig. 3.1. The spatial structure of the SVD modes for 1962–1993: The first modes of (a) zonal wind stress and (b) thermocline depth. (c) and (d) same as in (a) and (b) except for the second mode. Negative values are shaded. Units are non-dimensional. The contour intervals are 0.01.

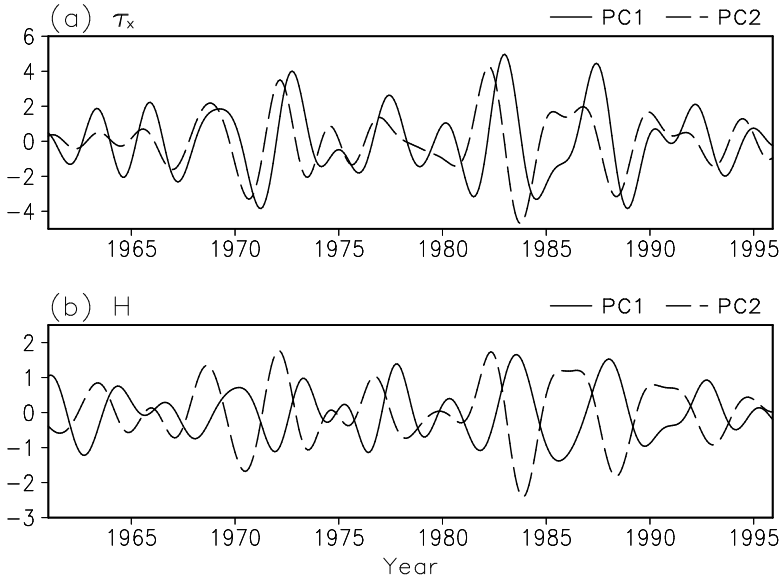

Fig. 3.2. The band–pass filtered (2–6 year) time coefficients of the SVD modes for 1962–1993: (a) the first (solid) and the second (dashed) modes for zonal wind stress anomaly, (b) same as in (a) but for thermocline depth anomaly.

3.2 Impact of wind stress variation on ENSO properties

3.2.1 Changes in ENSO properties in observational analysis

Analysis period is divided into two period (1962–1975; pre-shift period, 1980–1993; post-shift period) to find the phase change of ENSO according the climate shift. The lag covariance coefficient between the curl of zonal-mean wind stress (averaged over the western North Pacific) and the normalized NINO3 SST index (150°W–90°W, 5°S–5°N) is calculated to examine the relationship between the ENSO change and wind stress (Fig. 3.3a). The area was determined by considering the positive center in the second SVD mode (Fig. 3.1c). This mode generates the positive curl of the wind stress in this region.

Fig. 3.3b shows the lag covariance coefficient between the zonal-mean thermocline depth and NINO3 SST index. This coefficient represents the magnitude of the wind stress curl and thermocline depth associated with NINO3 SST index because this index is normalized into the standard deviation (Kang and Lau 1994). The positive wind stress curl exists in the western North Pacific before the mature phase of El Niño (warm phase of ENSO) both two periods. The maximum value is appeared before 4 months for the warm phase of ENSO during the pre-shift period. On the other hand, it is shown before 8

months during the post-shift period. The value in the pre-shift period ($1.2\times10^{-7}\mathrm{s}^{-1}$) is larger than that in the post-shift period ($0.8\times10^{-7}\mathrm{s}^{-1}$). The difference of the phase between the wind stress curl and ENSO phase is small (large) when the ENSO period is short (long) during the pre-shift period (post-shift period). The relationship of these two factors qualitatively agrees to the change of the ENSO period during two periods. This suggests that the change of wind stress over the western North Pacific is related to ENSO change during two periods.

Therefore, it is necessary to consider the effects of positive wind stress curl on ENSO period. The positive wind stress curl in the sub-tropics occurs negative thermocline depth anomalies and this is related to Ekman pumping process. ENSO transits to the next phase fast through the discharge of the heat content. The wind stress curl in the western North Pacific during pre-shift period is stronger than that during post-shift period. As mentioned earlier, there is fast transition from El Niño to La Niña during pre-shift period. The fast phase transition disturbs growth of El Niño by positive feedback mechanism (Bjerknes, 1969). El Niño which does not sufficiently grow has small amplitude and this agrees with the observational results. This process is confirmed in the Fig. 3.3b. The size of zonal-mean thermocline depth at equator is larger in the post-shift period than that in the pre-shift period. It is due to strong wind stress curl in the

pre-shift period. The time of the maximum value of the wind stress agrees to the time of the rapid reduction of the zonal-mean thermocline depth in the pre-shift period. This is the reason why the wind stress curl in the western North Pacific induces the fast discharge of the mass at the equator. On the other hand, the wind stress curl is weakened and the reduction of the thermocline depth becomes slow (or similar to normal year), relatively. After all, after the late-1970s, the period of ENSO is longer and intensity is stronger than before the late-1970s.

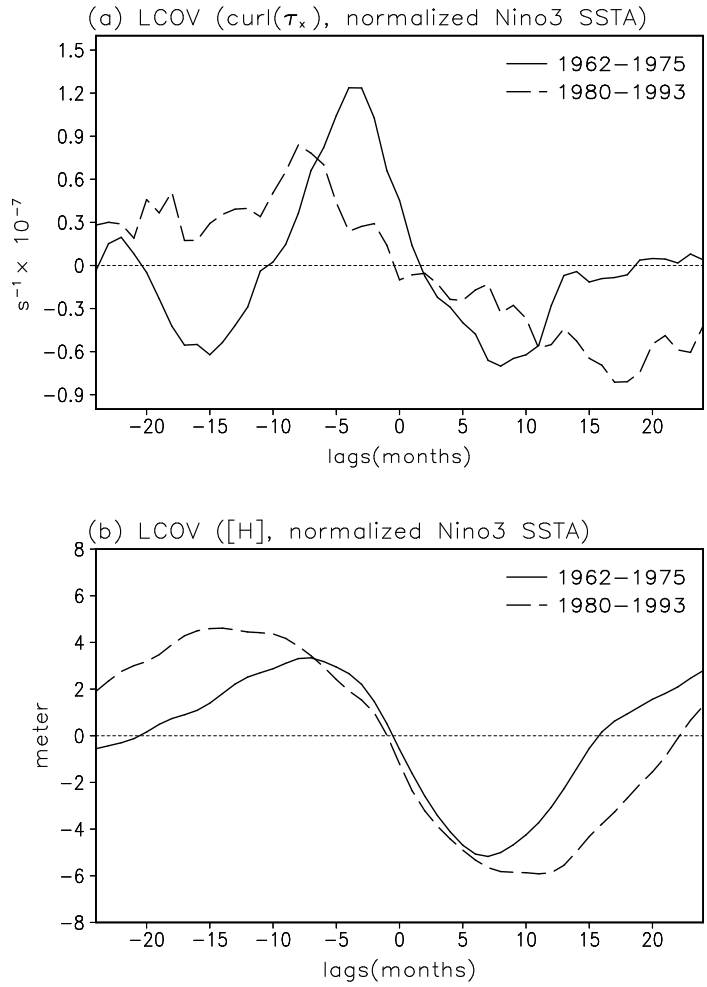

Fig. 3.3. (a) Lag covariance between the normalized NINO3 (150˚W–90˚W, 5˚S–5˚N) index and the curl of zonal wind stress anomaly averaged over western north Pacific (130˚E–170˚E, 5˚S–15˚N), (b) same as in (a) except for equatorial (5˚S–5˚N) zonal mean thermocline depth anomaly. Solid line represents during 1962–1975 (pre-shift period) and dashed line represents during 1980–1993 (post-shift period).

3.2.2 Verification using simple model

In the previous section, it was suggested that the strong wind stress curl decreases the thermocline depth over the tropical ocean and then generates the short period and weak intensity of ENSO. Simple atmosphere-ocean coupled model was conducted to understand details of physical mechanism and check the simulation of observational results.

a. model description and experiment organization

The ocean model in this dissertation includes the three baroclinic modes based on CZ model (Zebiak and Cane, 1987). Each of the three vertical baroclinic modes have phase speed ($C_n(n = 1,2,3)$), projection coefficient (P_n) (Table 3.1), and frictional scale of (γ_n). These values are derived from the vertical decomposition of equilibrium state over the central-tropical Pacific in the Levitus data (Yeh *et al*., 2001).

A term of $\gamma\frac{(T-T_{sub})}{H_1}$ related with subsurface temperature anomaly, which can affect the change of sea surface temperature, is calculated by using the Tropical Ocean Global Atmosphere-Tropical Atmosphere and Ocean Array (TOGA-TAO) data. The mean current data was derived from the ocean model after the steady-state (i.e., spinning up) using the wind stress data of Florida

State University. Atmospheric model is the similar to the statistical model used in the An and Wang (2000) and based on the SVD method (Kang and Kug, 2000; Yeh *et al*., 2001). That is, the wind stress data is reproduced through empirical method from SST in the ocean model. The monthly mean sea surface temperature and wind stress data is used to obtain the eigen-vector. The zonal and meridional wind stress vector of the first SVD mode is applied to conduct atmospheric model. This is the control experiment to examine for the effect of the wind stress over the western North Pacific (CTL experiment).

The empirical model which produces the wind stress is organized to examine response of the model according to the change of wind stress over the western North Pacific. The distribution of the wind stress produced in the model can be infered (Fig. 3.1c). To verify this, the simultaneous correlation coefficients of zonal wind stress anomaly with respect to the position (150°E, 9°N) in Fig. 3.1c (Fig. 3.4). The zonal wind stress similar to Fig. 3.4 can be represented using the Hermit function (Kang and Kug, 2002; An and Wang, 2000). This zonal wind stress is generated in proportion to the zonal-mean thermocline depth anomaly at the equator (5°S–5°N). This is to simulate the relationship between two variables during the pre-shift period in the Fig. 3.1.3a and b. This empirical model can be expressed as follows.

$$\tau_x(x,y,t) = \mu[H]_{5S}^{5N}(t)\left[\psi_0\left(\frac{y-y_0}{L_y}\right) - \psi_2\left(\frac{y-y_0}{L_y}\right)\right]\left[\exp\left(-\frac{(x-x_0)^2}{L_x{}^2}\right) - 0.2\right]$$

$$x_0 = 150^o, y_0 = 9^o, L_x = 20^o, L_y = 6^\circ$$

Where, ψ_0 and ψ_2 are 0th and 2nd Hermit function, respectively. x_0 is the longitudinal center and y_0 is the latitudinal center, respectively. L_x and L_y mean the longitudinal and latitudinal e-folding scale, respectively. $[H]_{5S}^{5N}$ represents the zonal-mean thermocline depth anomaly in the equator area (5°S–5°N). μ is the factor of coupling strength (0.6). This value is determined by having similar value as wind stress magnitude in observation, and Fig. 3.5 shows the spatial distribution of the wind stress derived from above equation. The experiment coupled this empirical atmosphere model and first SVD mode with ocean model is the WNP experiment. WNP experiment is constructed to check the period of ENSO generated by the first SVD mode varying with the wind stress over the western North Pacific. That is, WNP experiment is similar to pre-shift period and CTL experiment is similar to post-shift period. The design of the CTL and WNP experiment is in Table 3.2.

b. Model simulation results

Figure 3.6 shows the time series of NINO3 SST index obtained from CTL and WNP experiment. The intensity and period of ENSO is stronger and longer,

respectively, in the CTL experiment than that in the WNP experiment. The amplitudes are -2~+2°C in the CTL experiment and -1~+1.5°C in the WNP experiment. Fig. 3.7 is the wavelet result of the NINO3 SST index. The period of ENSO is about 5 year in the CTL experiment and 3.5 year in WNP experiment, respectively. This result confirms the role of the wind stress in the western North Pacific in the observation.

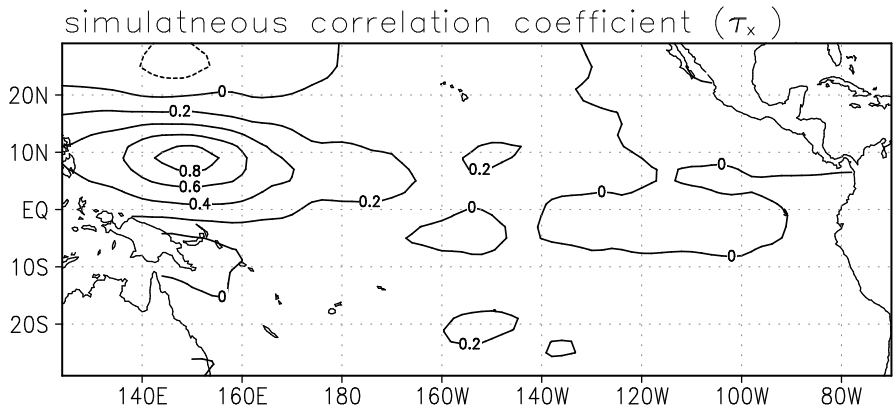

Fig. 3.4. One-point simultaneous correlation coefficient for the zonal wind stress anomaly with respect to the position (150˚E, 9˚N). The duration of data is 1961–97. The contour interval is 0.2.

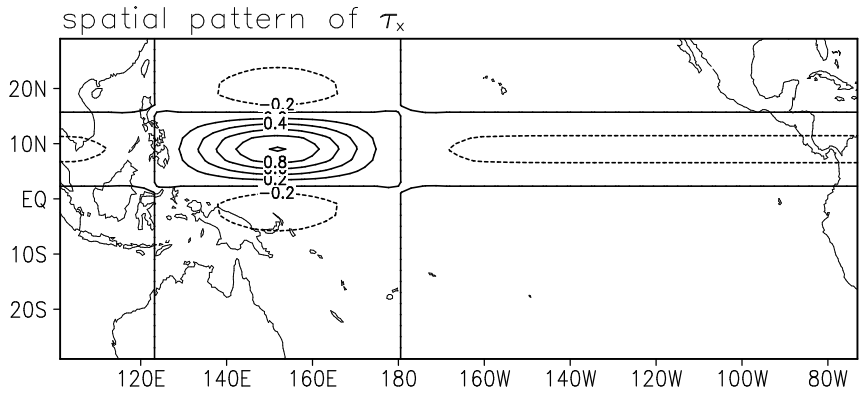

Fig. 3.5. Spatial pattern of the zonal wind stress anomalies in the idealized atmospheric model.

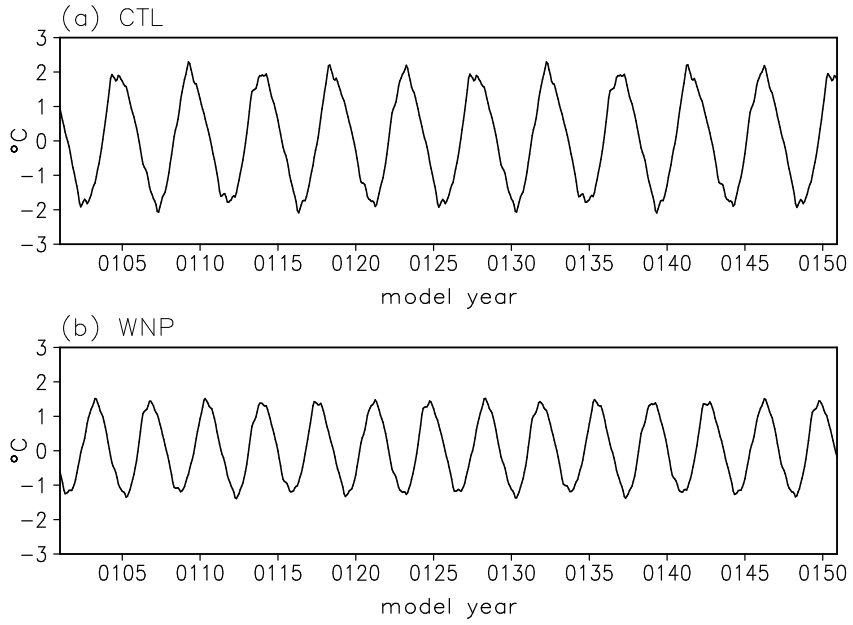

Fig. 3.6. The time series of the simulated NINO3 (150°W–90°W, 5°S–5°N) sea surface temperature anomaly for (a) CTL and (b) WNP experiments.

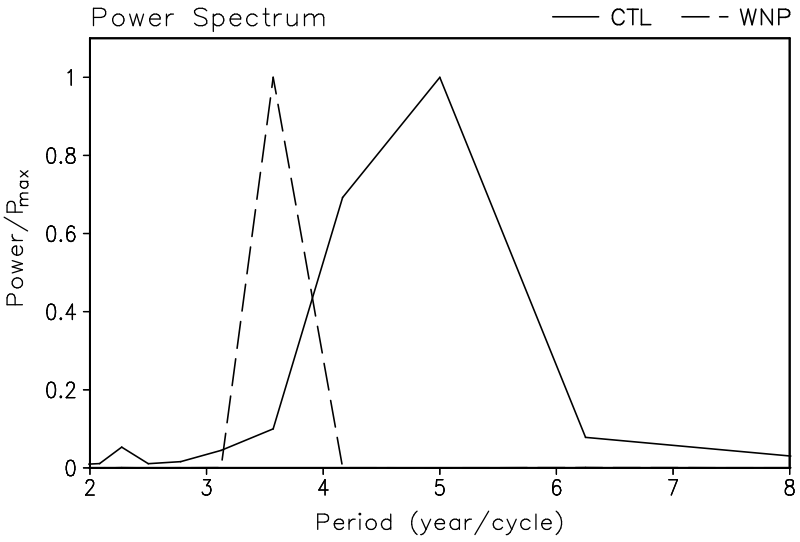

Fig. 3.7. Power spectrum of the simulated sea surface temperature averaged over NINO3 region (150˚W–90˚W, 5˚S–5˚N) for CTL and WNP experiments. For comparison, the power spectrums of the two experiments are divided by its maximum value.

Table 3.1. Parameter values for the ocean model. $A_n(z)$ are the vertical structures for the baroclinic modes, are derived from a density profile of Levitus data along the equator (160°E–140°W, Eq.).

	n=1	n=2	n=3
Phase speed (m/s): C_n	2.68	1.6	1.1
Projection coefficient : P_n	0.58	0.52	0.17
Frictional coefficient (in months): γ_n	30	23	18

Table 3.2 Experiment description. $\tau_x(x, y, t)$ means the empirical atmosphere model. See text for detail.

Experiment	Atmosphere model	Simulated period
CTL	First SVD mode	Post-shift (1980-1993)
WNP	First SVD mode + $\tau_x(x, y, t)$	Pre-shift (1962-1975)

CHAPTER 4

OCEAN STRATIFICATION VARIABILITY AND ENSO

4.1 Decomposition of vertical baroclinic mode associated with ocean stratification

In this section, details of the variability in the wind stress projection coefficient onto the oceanic baroclinic modes in the tropical Pacific in relation with the ENSO variability before and after the late-1970s was examined for the period 1958-97.

Figure 4.1 shows the longitudinal distribution of the projection coefficients of the wind stress onto the three oceanic baroclinic modes (see section 2.2.2, hereafter, $P_n(x, y)$, n = 1,2,3) averaged over the region (5°S–5°N) for the entire

analyzed period 1958–97. The most striking feature is that, in the western equatorial Pacific, P_1 is larger than P_2 and P_3, reflecting the zonal structure of the thermocline. In other words, the wind stress forcing over the western equatorial Pacific mostly projects onto the first oceanic baroclinic mode. In the eastern tropical Pacific, on the other hand, P_2 and P_3 are larger than P_1. As pointed out by Eriksen (1988), the wind stress forcing projects most efficiently onto the higher baroclinic modes when the thermocline depth is shallow in the eastern Pacific. In the central equatorial Pacific, the first and the second oceanic baroclinic modes tend to capture similar input of wind stress forcing. The result is similar to that obtained by Dewitte *et al*. (1999) who calculated the projection coefficients using a high-resolution ocean general circulation model (OGCM) simulation for 1985–94. Note that Dewitte *et al*. (1999) calculated the projection coefficients along the equator rather than off the equator.

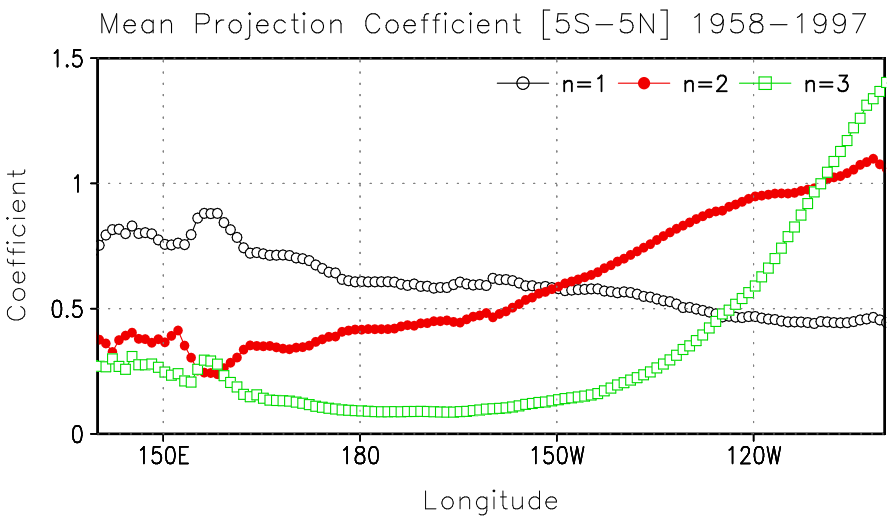

Fig. 4.1. Longitudinal distribution of mean projection coefficient (P_n) over the region of 5°S–5°N for the first three baroclinic modes (n=1, black; n=2, red; and n=3, green) during the period 1958–1997.

Figure 4.2a displays the time series of P_1 averaged over the western equatorial Pacific. The P_1 in the western equatorial Pacific shows considerable variability on interannual-to-decadal timescales. In particular, the variability of P_1 is characterized by a significant change before and after the mid-1970s. In details, the P_1 gradually decreases before the mid-1970s and then the P_1 abruptly increases after the mid-1970s. 8–year running mean of P_1 (red line in Fig. 4.2a) clearly indicates that since the mid-1970s the P_1 gradually increases, indicating that the wind stress forcing projecting onto the first oceanic baroclinic mode experiences a shift before and after the mid-1970s. Figure 4.2b is the same as in Fig. 4.2a except but the time series of P_2 over the eastern equatorial Pacific. The variability of P_2 is somewhat different compared to the P_1 over the western equatorial Pacific, that is, it is dominated by a modulated seasonal cycle. On the other hand, an 8-year running mean time series (red line in Fig. 4.2b) show that there exist decadal changes of P_2 around the early-1970s. Comparing to the variability of P_1, an increase of P_2 over the eastern equatorial Pacific starts a little bit earlier than the mid-1970s. The low-frequency of P_1 and P_2 variability in Fig. 4.2a and b indicate that changes in the wind stress forcing projecting onto the first and second oceanic baroclinic modes may be associated with the well-known climate shift of tropical Pacific around the mid-1970s.

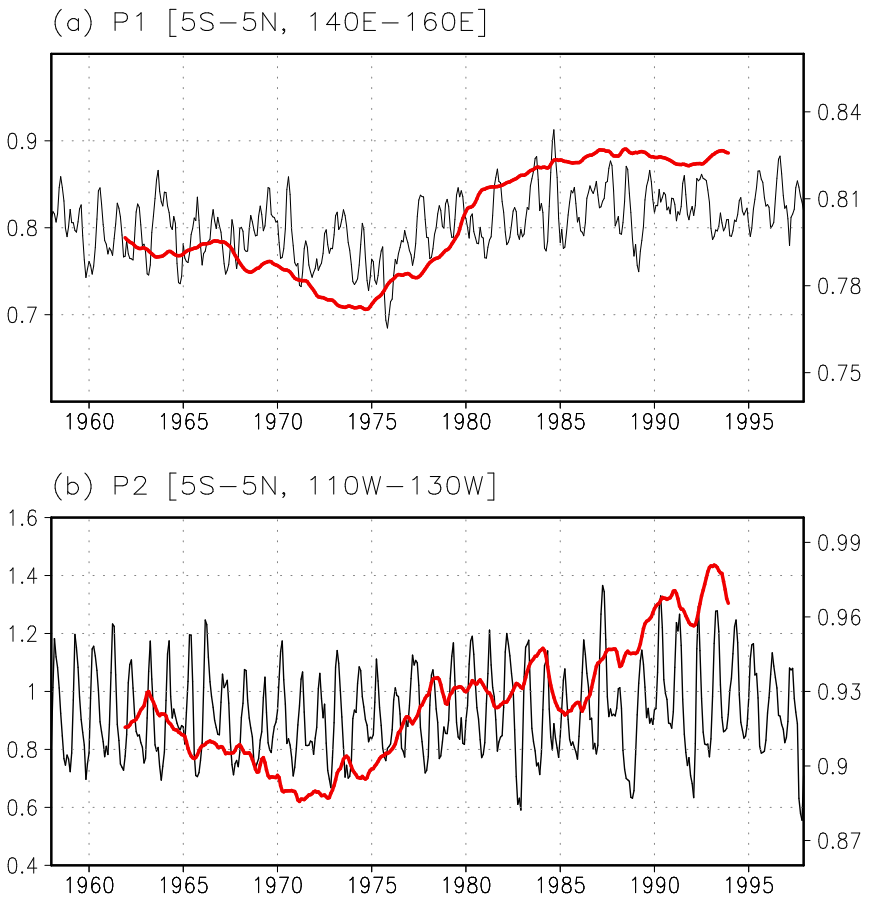

Fig. 4.2. Time series of (a) P_1 over the western equatorial Pacific and (b) P_2 over the eastern equatorial Pacific. Red line indicates 8-yr running mean

4.2 Contribution of vertical baroclinic mode to ENSO evolution

4.2.1 Relationship between vertical baroclinic mode and ENSO

So far, this dissertation has analyzed the variability of P_n in the regions where the values of P_n peaks, namely in the western equatorial Pacific for P_1 and the eastern equatorial Pacific for P_2. However, surface momentum forcing over the equatorial Pacific is larger in the central equatorial Pacific than the western and eastern equatorial Pacific, which is illustrated by the analysis of zonal wind stress standard deviation (Fig. 4.3a). One can find that a center of maximum zonal wind variance is located in the central equatorial Pacific (170°E–170°W, 7°S–3°N) around the dateline; therefore, it is necessary to examine the variability of P_n averaged over the central equatorial Pacific. Note that the P_n quantifies the amount of momentum flux that projects on a particular baroclinic mode in the central equatorial Pacific where the first and the second oceanic baroclinic modes are dominant and have comparable contributions (see Fig. 4.1).

In addition, the variability of the zonal wind stress forcing over the central equatorial Pacific is highly correlated with the ENSO variability, which further

enables to examine the relationship of P_n with the ENSO variability. Figure 4.3b further displays the regressed zonal wind stress against the NINO3 SST. The maximum regressed zonal wind stress (Fig. 4.3b) is observed in the central equatorial Pacific where the surface zonal momentum forcing is the largest as shown in Fig. 4.3a. A simultaneous correlation coefficient between the zonal wind stress anomalies over the central equatorial Pacific and the NINO3 SST index is 0.64 (Fig. 4.3c), which is statistically significant at 95% confidence level. Furthermore, it is found that a maximum correlation coefficient between the zonal wind stress anomalies and the NINO3 SST index (r=0.69) is observed at the one-month lead time, indicating that the variability of zonal wind stress forcing over the central equatorial Pacific slightly leads the ENSO variability.

Figure 4.4 displays the lead-lagged relationship between the time series of P_1 and P_2 averaged over the region of the central equatorial Pacific and the NINO3 SST index, respectively. It is clear that the wind stress projecting onto the first two baroclinic modes acts differently to the development of ENSO. Figure 4.4 indicates that P_1 is ahead the NINO3 SST index at 1~2 months lagged time, which is consistent with the relationship of zonal wind stress variability over the central equatorial Pacific and ENSO variability. That is, the wind stress projecting onto the first oceanic baroclinic mode over the central equatorial Pacific preliminary forces ENSO on a developing phase. The

eastward propagating Kelvin wave, which is due to the first baroclinic mode forcing, can impact SST in the eastern equatorial Pacific through vertical advection with a delay of 1 to 2 months (that corresponds to the traveling from west to east at the speed of the first baroclinic mode).

On the other hand, P_2 is behind ENSO, which indicates that the wind stress projecting onto the second oceanic baroclinic mode responses to ENSO on the growing and decaying phase. This indicates that high-order oceanic baroclinic modes can control the ENSO amplitude and life cycle. As ENSO develops, the thermocline flattens in the central tropical Pacific and concurrently deepens in the eastern equatorial Pacific. This can lead an increased energy distribution toward the high-order (here, second) oceanic baroclinic mode in the central equatorial Pacific.

In addition to the relationship with ENSO variability, it is valuable to examine the relationship of the variability of P_1 and P_2 in the central equatorial Pacific. A simultaneous correlation coefficient between P_1 and P_2 for the period 1958-97 is 0.04, indicating that the variability of P_1 has little relationship with the variability of P_2. It is also true that P_1 has no significant correlation with P_3. A simultaneous correlation coefficient between P_1 and P_3 for the period 1958-97 is -0.06. That is, the surface zonal wind stress projecting onto the gravest (i.e., first) and high-order (i.e., second and third) oceanic

baroclinic modes is nearly independent in the central equatorial Pacific.

However, it is found that such a relationship changes with time, in particular, before and after the mid-1970s in relation to the decadal changes in the ENSO properties. The variability of P_1 is positively correlated with that of P_2 before the late-1970s. In contrast, P_1 and P_2 are negatively correlated with each other after the late-1970s (Table 4.1). Such a reversed relationship before and after the late-1970s is also true between P_1 and P_3. On the other hand, the relationship between P_2 and P_3 is not significantly changed before and after the late-1970s. Table 4.1 summarizes the correlation coefficients between the P_n (n=1, 2, 3) before and after the late-1970s. The results indicate that the surface wind stress over the central equatorial Pacific constructively and destructively projects onto the gravest and high-order baroclinic modes before and after the late-1970s, respectively. This indicates that the way in whcih wind stress projecting onto the oceanic baroclinic modes over the central equatorial Pacific is significantly changed in the 1970s climate shift. Furthermore, one may argue that the relationship of P_1 and P_2 over with ENSO is also changed before and after the late-1970s.

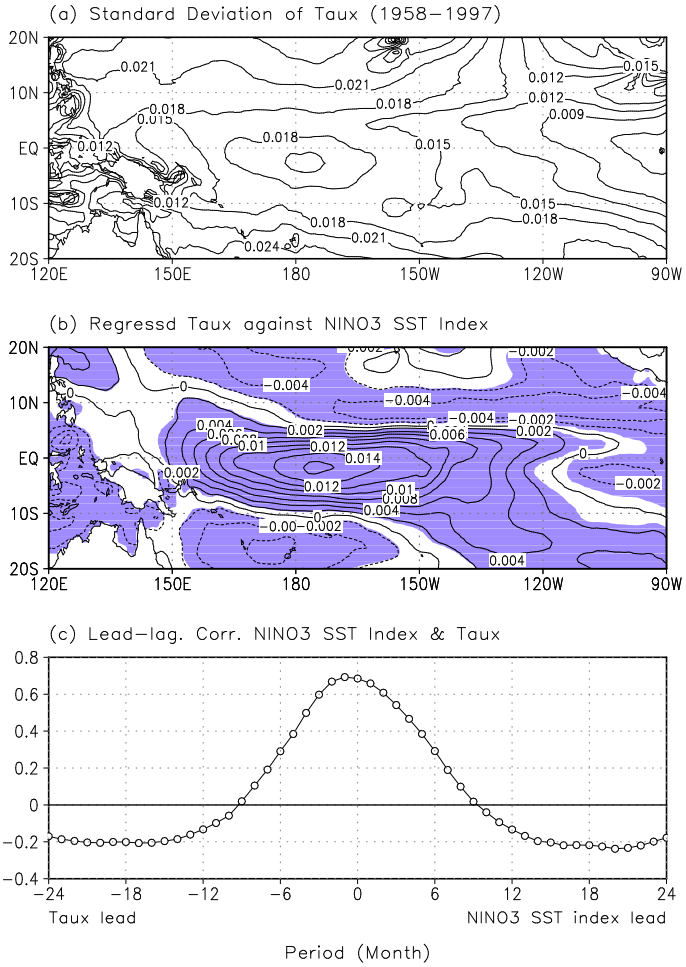

Fig. 4.3. (a) Standard deviation of the zonal wind stress, (b) regressed zonal wind stress against the NINO3 SST index. Shaded areas are significant at 95% confidence level. (c) Lead-lagged correlation coefficient between the NINO3 SST index and the zonal wind stress anomalies over the central equatorial Pacific (170°E–170°W, 7°S–3°N) and during the period 1958–1997.

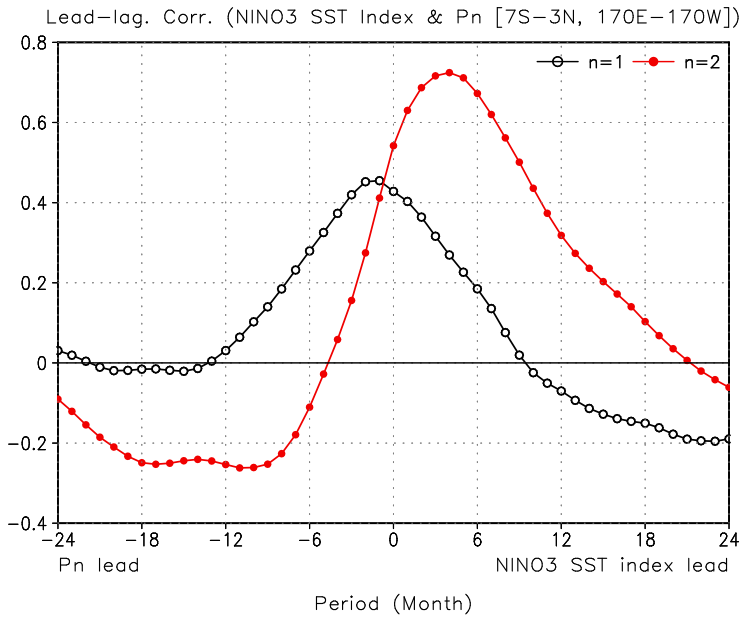

Fig. 4.4. Lead-lagged correlation coefficients between the NINO3 SST index and the time series of P_n over the central equatorial Pacific. (n=1 (black open circle) and n=2 (red closed circle)).

Table 4.1 Correlation coefficient between the projection coefficients of the different baroclinic modes during the periods 1958–1975 and 1980–1997.

Correlation coefficient	P_2		P_3	
	1958-1975	1980-1997	1958-1975	1980-1997
P_1	0.53**	-0.3*	0.36**	-0.33*
P_2	–	–	0.85**	0.94**

** Significance at a 95% confidence level.* Significance at a 90% confidence level.

4.2.2 Decadal changes in the relationship of ENSO–vertical baroclinic mode

Figures 4.5 is the same as in Fig. 4.4 except for over the two periods before and after the late–1970s, respectively. Before the late–1970s, the P_1 is slightly behind the NINO3 SST index, which is somewhat different from its position in Fig. 4.4. This indicates that the wind stress projecting onto the first baroclinic mode over the central equatorial Pacific, which is associated with the eastward propagating Kelvin waves, does not actively participate to ENSO at the developing stage before the late–1970s. On the other hand, P_2 is behind the NINO3 with 4–5 months lagged time (Fig. 4.5a), which is similar to Fig. 4.4, indicating that the ENSO variability leads the wind stress projecting on the second oceanic baroclinic mode over the central equatorial Pacific.

After the late–1970s, in contrast, the wind stress projecting onto the first oceanic baroclinic mode preliminary forces ENSO on the developing phase (Fig. 4.5b). One may find that the variability of P_1 leads the NINO3 SST index by 4~5 months. On the other hand, the wind stress projecting onto the second oceanic baroclinic mode responses to ENSO on the growing and decaying phase. This reflects the change in equatorial wave dynamics through the forcing of baroclinic modes from before and after the late–1970s.

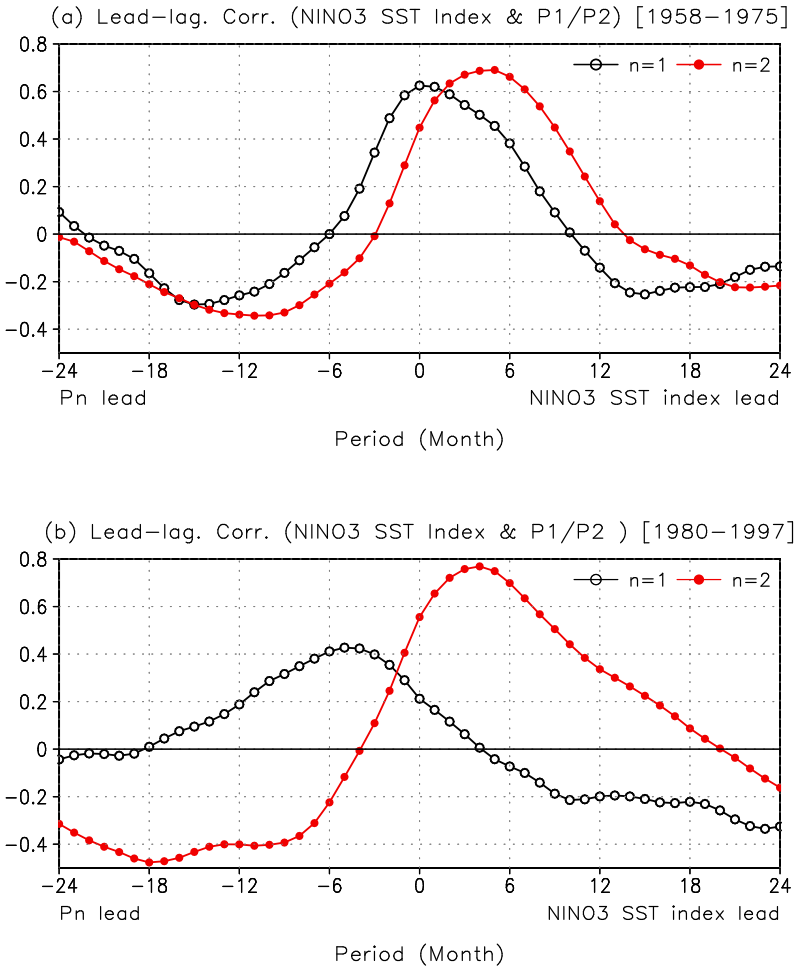

Fig. 4.5. Lead-lagged correlation coefficients between the NINO3 SST index and the time series of P_1 (black open circle) & P_2 (red closed circle) over the central equatorial Pacific during the period (a) 1958–1975 and (b) 1980–1997.

The interannual variability associated with the wind stress projection coefficients of the first three baroclinic modes experienced significant changes between before and after the mid–1970s was shown. These changes reflect changes in ENSO feedback processes because each mode has a specific effect on the coupled instabilities of the equatorial Pacific system through their meridional scale of variability (i.e., the higher is the order of the baroclinic mode, the finer is the meridional scale), their propagation characteristics, and their contribution to the momentum flux. Whereas most studies have focused on changes in stratification on longer timescales (Moon *et al*. 2004; Dewitte *et al*. 2007), the analysis of these changes on an interannual timescale and their relations with ENSO offer an alternative view for interpreting changes in ENSO properties on decadal timescales. In particular, it allows for estimation of the coupling efficiency associated with each baroclinic mode in the development of ENSO.

The first three baroclinic modes were selected here because of their propagating characteristics and their significant contributions to ENSO variability (Dewitte *et al*. 1999). The summed contribution of the higher-order modes, although trapped within the mixed layer, can also have a significant contribution to the interannual variability in the tropical Pacific (Dewitte *et al*. 1999). In particular, if the wind stress forcing onto the high-order baroclinic

modes is weakened after the late-1970s, it may be argued that changes in the equatorial wave dynamics, associated with the variability in the first three oceanic baroclinic modes, is a key process involved in the change in the ENSO variability.

4.3 Contribution of vertical baroclinic mode to ENSO spatial pattern

4.3.1 Recent changes of SST in the warm pool

a. Define and characteristics of warm pool region

Western Pacific warm pool region (hereafter, warm pool), where the wind stress variation is small, is associated with ENSO (out of phase with El Niño). This region where the SST is above 28°C encompasses the western tropical Pacific. Figure 4.6a displays the climatological mean SST of HadISST data during the winters (October, November, December, January, and February) of 1958-2004. It is evident that the warm pool extends more to the southwestern tropical Pacific and the maximum SSTs are confined to the South Pacific Convergence Zone (SPCZ) between 150°E and 170°W. The western Pacific warm pool is defined as the region [120°E–170°W, 20°S–20°N] in this dissertation.

The 47-yr monthly mean SST time series are shown in Fig. 4.6b. Figure 4.6b agrees with findings from previous studies showing that the warm pool SST has gradually increased over the past five decades (Sun 2003; Wang and Mehta 2008; Cravatte *et al*. 2009; Kim and An 2011).

Figure 4.7 shows the standard deviation of SST anomalies for the period

1958–2004. The maximum standard deviation (about 1°C) is observed in the eastern part of the warm pool. In contrast, the SST variability in the western part of the warm pool is weak and its standard deviation is less than half of the maximum standard deviation in the eastern part of the warm pool. That is, SST anomaly variability in the warm pool region is characterized by an east-west contrast in terms of their magnitude.

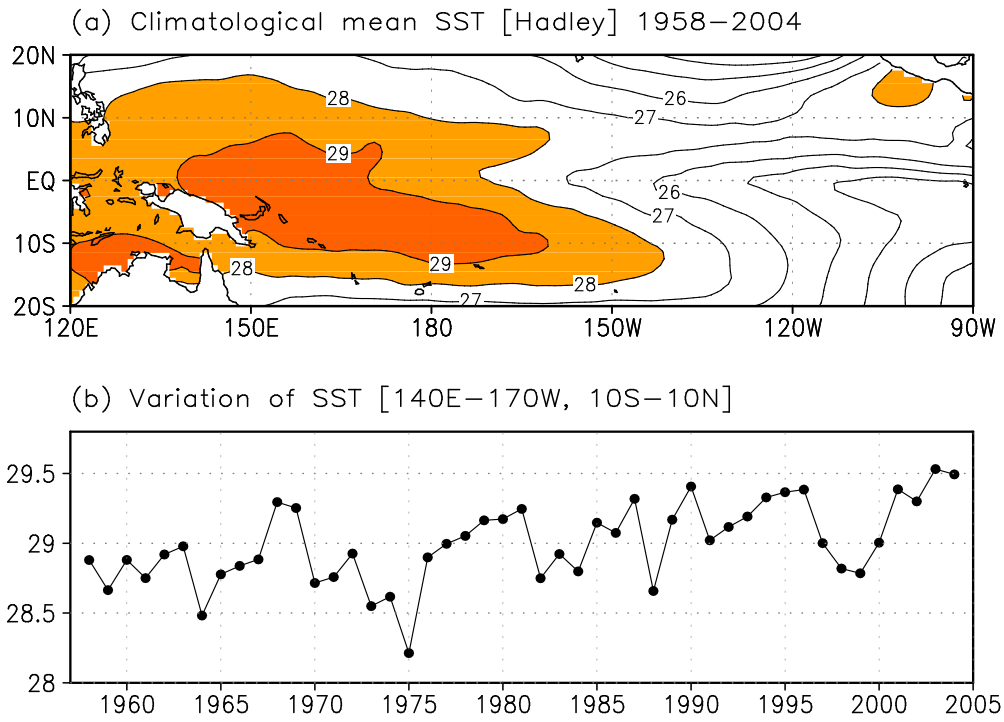

Fig. 4.6. (a) Climatological mean sea surface temperature (shades area are exceed 28°C) and (b) variation of sea surface temperature over the region [140°E–170°W, 10°S–10°N] in HadISST for the period 1958–2004.

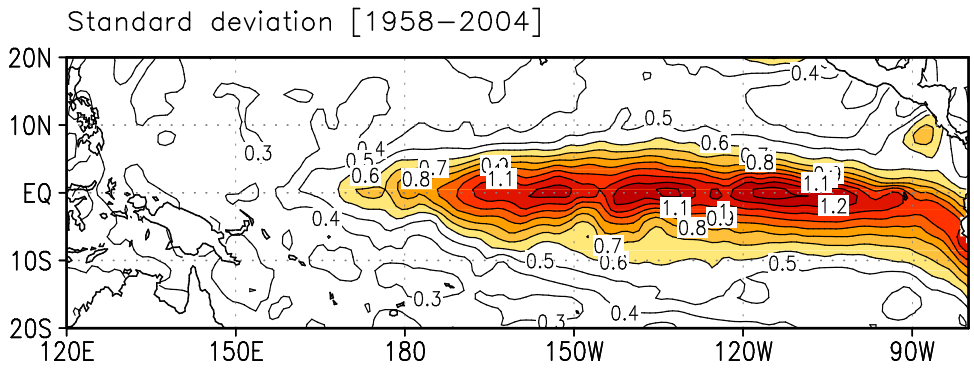

Fig. 4.7. Standard deviation of sea surface temperature anomalies for the period 1958–2004.

b. EOF analysis

To further examine the details of SST anomaly variability in the warm pool, an EOF analysis was performed. Fig. 4.8a and b display the first and second EOF modes of SST anomaly in the warm pool, which account for 36.1 % and 20.5 % of the total SST anomaly variance, respectively. The first two EOFs are well separated from the rest of the modes according to the Eigen value criterion of North *et al*. (1982) and represent robust features of SST anomaly variability in the warm pool region. The spatial structure of the first EOF mode is dominated by positive anomalies in the western warm pool and negative anomalies in the eastern warm pool, respectively. Usually, the warm pool is characterized by a uniform mean SST (Fig. 4.6), whereas variability of the first EOF mode of SST represents a zonal contrast of SST anomalies within the warm pool. This is clearly revealed in Fig. 4.8c by the dipole pattern in the zonal profile of the EOF first mode structure averaged between 5°S and 5°N. Variations of the warm pool SST to west of 180°E are out of phase with those to the east. As for the EOF2, its SST anomaly structure is characterized by a horseshow-like feature, in which the maximum of SST variance is located in the central-to-eastern parts of the warm pool and extend northeast and southeast into the both hemispheres. The zonal profile of the EOF2 structure in the equatorial region (5°S–5°N) is dominated by a center of action near the

central Pacific (Fig. 4.8c).

Figure 4.9a and b shows the first and second mode of principal components (PCs) of EOF. The EOF PC1 is characterized by a trend that evolves from negative values before the mid-1980s to positive values afterward. In view of the spatial pattern of EOF first mode (Fig. 4.8a), the first mode of PC represents a warming trend in the warm pool during the recent decades, which seems to be consistent with the time series of mean SST averaged in the warm pool (120°E–170°E, 10°S–10°N).

According to previous studies, the warm pool SST has warmed over the last century in a manner similar to the global mean surface air temperature (Sun 2003). Sun (2003) argued that such a similarity indicates that the warming trend in the warm pool SST could be a result of global warming. Therefore, the leading SST variability identified by the EOF1 SST mode, represents the influence of global warming to the warm pool. EOF1 and its PC together indicate that the warming in the warm pool is accompanied with an enhancement of the zonal SST gradient within the warm pool, which suggests the western warm pool has become warmer while the eastern warm pool becomes cooler during the recent decades. More details will be shown later.

In contrast, the EOF2 PC (Fig. 4.9b) is dominated by decadal-scale variations. A power spectrum analysis indicates that the EOF PC2 is characterized by a

spectral peak around 11–12 years. Furthermore, it is noticed that the spectral density of EOF PC2 is different from that of the NINO3 (210°E–270°E, 5°S–5°N,) SST index or NINO3.4 (190°E–240°E, 5°S–5°N) SST index, which are used to represent the conventional ENSO. The spectral density of NINO3 and NINO3.4 index is dominant by interannual timescales with a spectral peak around 3–4 years. Therefore, these results indicate that the warm pool variability as associated with the EOF2 is distinguished from the conventional ENSO. The correlation coefficients between the NINO3, NINO3.4, NINO4 (160°E–210°E, 5°S–5°N) SST index and the EOF PC1 and PC2s, respectively, are shown in Table 4.2. It is evident that the EOF PC2 is most correlated with the NINO4 SST index. This result indicates that the EOF2 mode of warm pool SST variability is associated with to some extent the SST variability in the central equatorial Pacific (i.e., NINO4 region). The correlation coefficient between mean sea surface temperature averaged over the warm pool [120°E–170°E, 10°S–10°N] and EOF PC1 is 0.87, and EOF PC2 is 0.45.

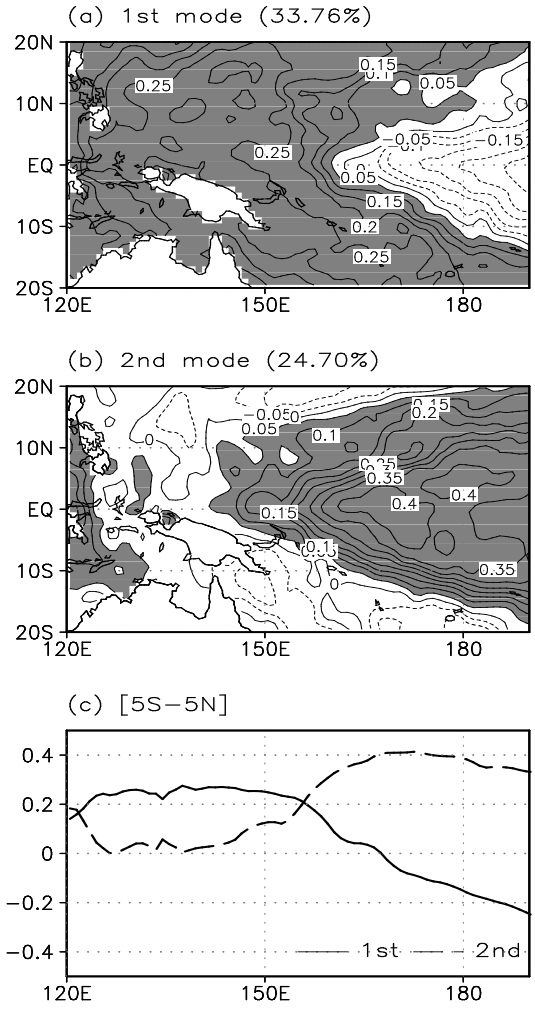

Fig. 4.8. Eigen vectors of normalized sea surface temperature anomalies (a) the first mode, (b) the second mode, and (c) meridional mean [5°S–5°N] of the first mode (solid line) and the second mode (dashed line) for the period 1958–2004. Positive values are shaded.

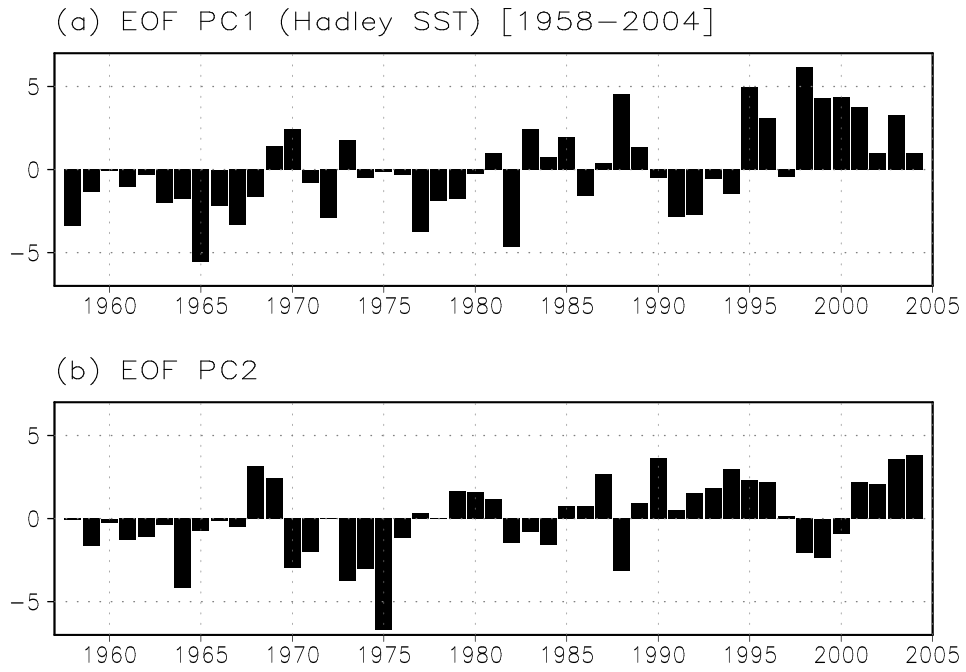

Fig. 4.9. Time series of EOF SST (a) PC1 and (b) PC2.

Table 4.2. Correlation coefficients between EOF PC1 & PC2 and NINO index during the period 1958–2004.

	EOF PC1	EOF PC2
NINO3	-0.49	0.40
NINO3.4	-0.59	0.51
NINO4	-0.50	0.77

The regression analysis for the tropical Pacific SST anomalies against with the EOF PC1 and PC2 was performed to identify the basin-wide SST anomaly pattern associated with these two EOFs. The results are shown in Fig. 4.10. The regions where the regressions are significant at the 95% level are shaded. The figure shows that the EOF1 is associated with a significant warming in the western tropical Pacific and cooling in the central Pacific. This indicates that the warming trend of warm pool represented by the SST EOF1 mode is accompanied with a La Niña-like SST pattern in the tropical Pacific basin. Considering the trend in the EOF PC1 (Fig. 4.9a), Fig. 4.10 further implies that the mean SST changes toward a La Niña-like pattern with warming in the west and cooling in the east during the recent decades. It is noteworthy that it is also related to an enhancement of zonal gradient of mean SST in the tropical Pacific (Karnauskas *et al*., 2009).

Previous studies have shown that the twentieth-century SST trend associated with global warming is similar to a La Niña-like SST pattern in the tropical Pacific (Cane *et al*. 1997, Vecchi and Soden 2007). Such a La Niña-like SST pattern also has a tendency to increase the mean SST gradient across the equatorial Pacific. An "Ocean dynamical Thermostat" mechanism was proposed to explain why the global warming should lead to an increase in the zonal temperature gradient across the equatorial Pacific (Clement *et al*. 1996,

Cane *et al*. 1997, Seager and Murtugudde 1997, Vecchi and Soden 2007). Based on these previous studies and our results, we conclude that the SST EOF 1st mode reflects the changes in the mean SST of the warm pool in response to global warming.

The basin-wide SST anomalies regressed with the EOF PC2 (Fig. 4.10b) are characterized by maximum SST anomalies in the central equatorial Pacific, which is consistent with Table 4.2 that the EOF PC2 is highly correlated with the NINO4 SST index. The regressed pattern is very similar to the SST anomaly pattern of CP El Niño (Larkin and Harrison 2005, Ashok *et al*. 2007, Kao and Yu 2009, Kug *et al*. 2009). It is noticed that positive values of the EOF PC2 became dominant after the mid–1980s (Fig.4.9b).

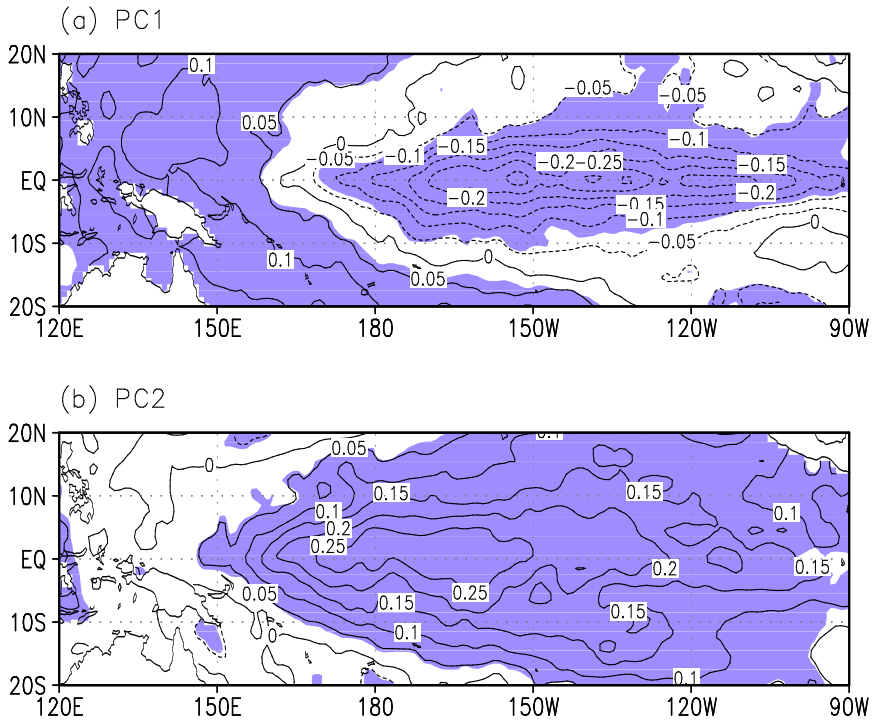

Fig. 4.10. Regressed sea surface temperature anomalies against EOF (a) PC1 and (b) PC2. Shaded areas are significant at 95% confidence level.

In addition to the associated SST anomaly pattern, it is useful to identify the upper-ocean structure associated with the EOF1 and EOF2. Fig. 4.11 shows the vertical cross sections of ocean temperature regressed to the EOF PC1 and PC2 along the equator. It shows that the subsurface structures for these two EOFs are quite different. For the EOF1, out-of-phase temperature anomalies in the subsurface ocean appear on both sides of the tropical Pacific basin, which may be associated with changes in the east-west slope of the thermocline. This structure also reflects a La Niña-like pattern with a surface warming in the west and cooling in the east. The maximum value of both positive and negative subsurface anomalies is observed at the depth of 80–150m. In particular, a tilting structure of negative subsurface anomalies in the eastern tropical Pacific implies that the negative SST anomalies in the eastern tropical Pacific (see Fig. 4.8a) are attributed to the upwelling of colder water (Clement *et al*. 1996, Cane *et al*. 1997). Therefore, the subsurface ocean dynamics play a role in inducing the changes in mean SST to a La Niña-like pattern, which is related to the SST EOF1 mode of variability in the warm pool during the recent decades. On the other hand, the subsurface temperature anomalies regressed with the EOF PC2 is characterized by an out-of-phase structure in the vertical direction, in particular in the western and central equatorial Pacific (Fig. 4.11b). This is in contrast with the regressed temperature anomalies against with the

EOF PC1 in which the out-of-phase structure is significant in the east-west direction. The variability of SST EOF2 mode in the warm pool is significantly associated with the temperature anomalies around the depth of 150 m in the western and central equatorial Pacific. Positive subsurface anomalies are located from the surface to the depth of 100 m, which is consistent with a warm SST in the central equatorial Pacific as shown in Fig. 4.10b.

EOF PC2 of warm pool SST and projection coefficient over the western Pacific region has highly related each other. In particular, the simultaneous correlation coefficient between EOF PC2 and P_1 is 0.7 and between EOF PC1 and P_2 is -0.4. This result is associated with relationship between EOF PC1/2 and NINO index (Fig. 4.12).

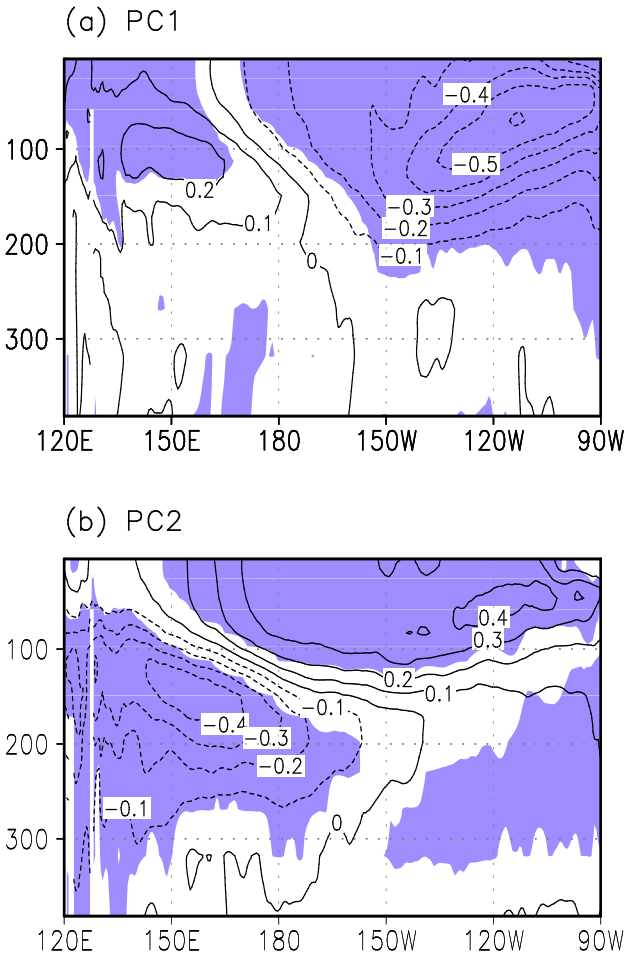

Fig. 4.11. Same as in Fig. 4. 10 except for the vertical ocean temperature..

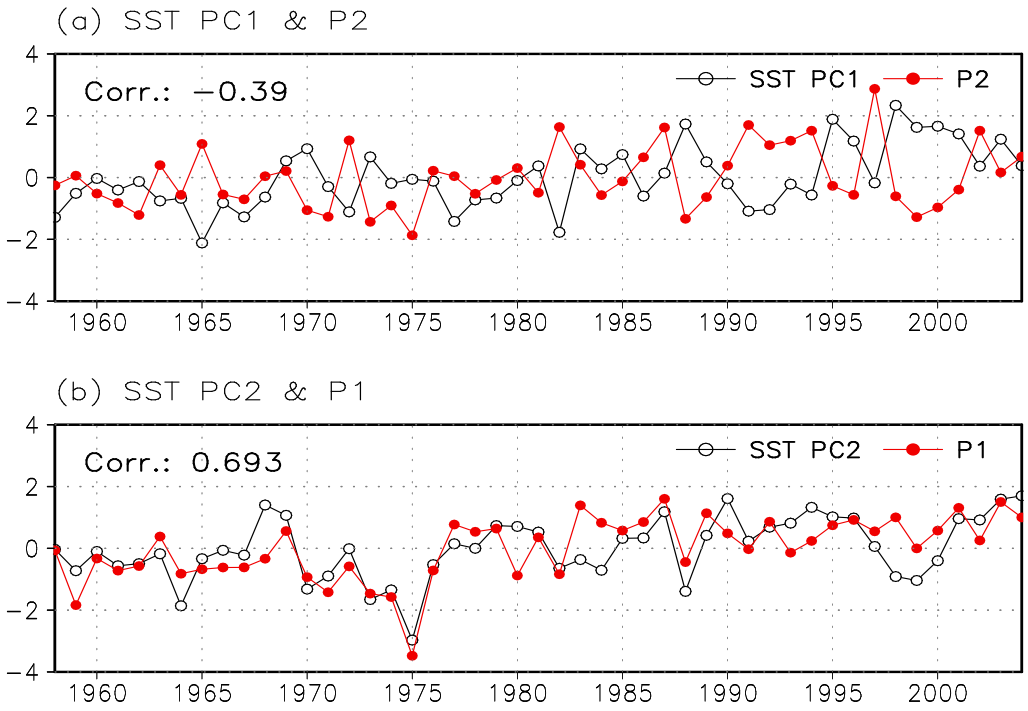

Fig. 4.12. Time series (a) EOF SST PC1 and P_2, and (b) EOF SST PC2 and P_1.

To describe the variability of the warm pool region in the western Pacific, WP index was constructed by averaged SSTA over the warm pool region [140°E–170°W, 10°S–10°N] where the core of the warm pool region SST was above 28°C using unfiltered monthly anomaly data (Fig. 4.13a). Hereafter, this variation of anomalies will be referred to as the warm pool index (WPI).

Figures 4.13a shows a significant warming trend during 1958–2004. The WPI can be divided into three sub-periods, each with a different mean warm pool SST: 1958–76 (hereafter, W1 period), 1977–88 (hereafter, W2 period), and 1989–2004 (hereafter, W3 period). The anomalous mean WPI in the three periods are -0.19°C, 0.02°C and 0.20°C, respectively. It is obvious that the mean WPI during the W1 period exhibits relatively cooler than the mean WPI during the W2 period and W3 period, especially when compared to the WPI during the W3 period. Compared to the W3 period, the WPI during the W2 period is characterized by the variations of anomalous warm and cool WPI on interannual timescales, therefore, this period could be considered as a transition phase between the two sub-periods, W1 period versus W3 period. In addition, Figs. 4.13b and c show the difference of mean SST between two periods of W3 period and W1 period versus W2 period and W1 period, respectively, in the warm pool region. One may find that the warming of warm pool SST from the W1 period to the W3 period is more evident compared to the W2 period.

Hereafter, W1 period (1958–76) and W3 period (1989–2004) will be compared to examine how changes in the warm pool SST associated to baroclinic mode fluctuations influence tropical Pacific SST.

Figure 4.14 displays the regressed sea surface temperature to the WPI for the period 1958-76 and 1989-2004, respectively. The spatial pattern of regressed SST is quite different between the two sub-periods. The regressed SST has a warming in the central and eastern tropical Pacific during W1 period. On the other hand, the regressed SST shows the maximum valued over the central Pacific near the date-line, and the location of the maximum center in regressed SST is shifted westward during W3 period. The regressed zonal wind stress against the WPI also shows that the location of maximum center is westward shift from W1 period to W3 period (Fig. 4.15).

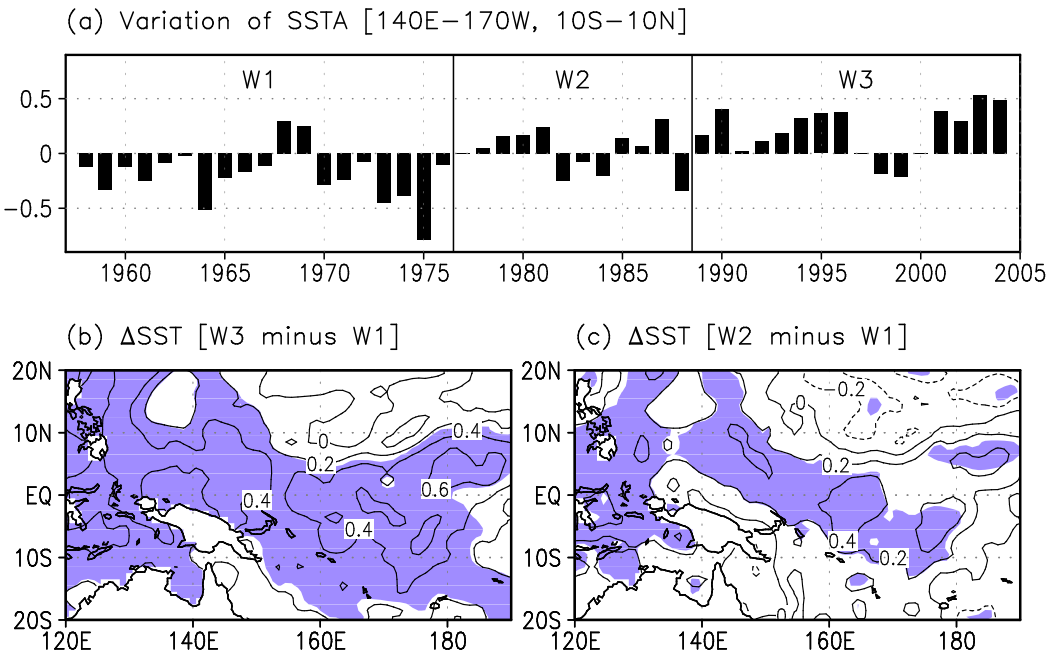

Fig. 4.13. Time series of (a) sea surface temperature anomalies over the region [140°E–170°W, 10°S–10°N] based on the HadISST data, (b) Mean SST difference between W3 [1989–2004] and W1 [1958–76] (W3 minus W1), and (c) Mean SST difference between W2 [1977–88] and W1 [1958–76] (W2 minus W1) based on the HadISST data. Shading denotes a statistical significance at 95% confidence level.

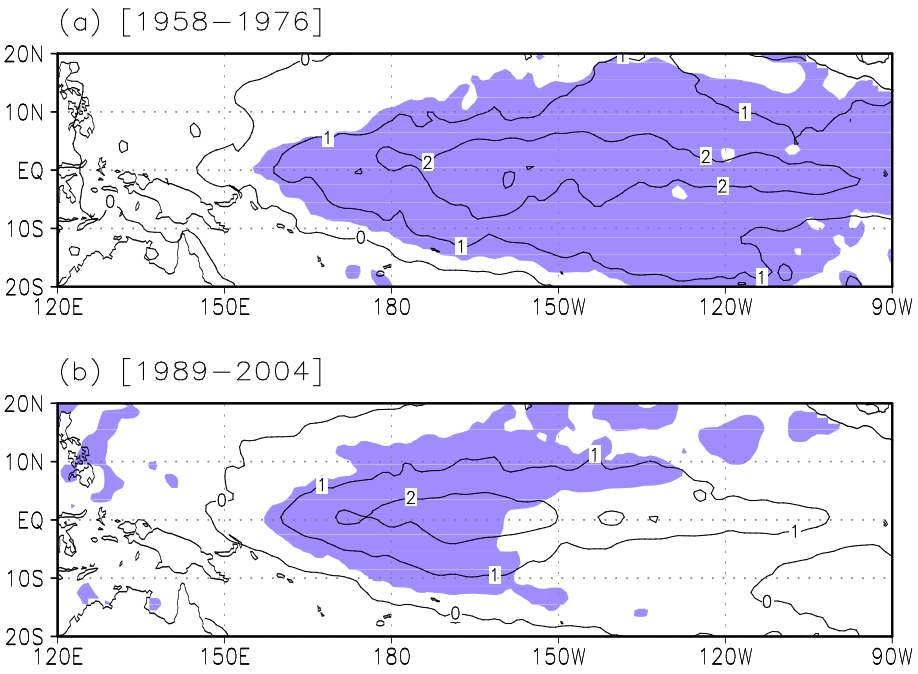

Fig. 4.14. Regressed sea surface temperature anomalies against the WPI during for the (a) W1 period [1958-1976] and (b) W3 period [1989-2004]. Shaded areas are significant at 95 % confidence level.

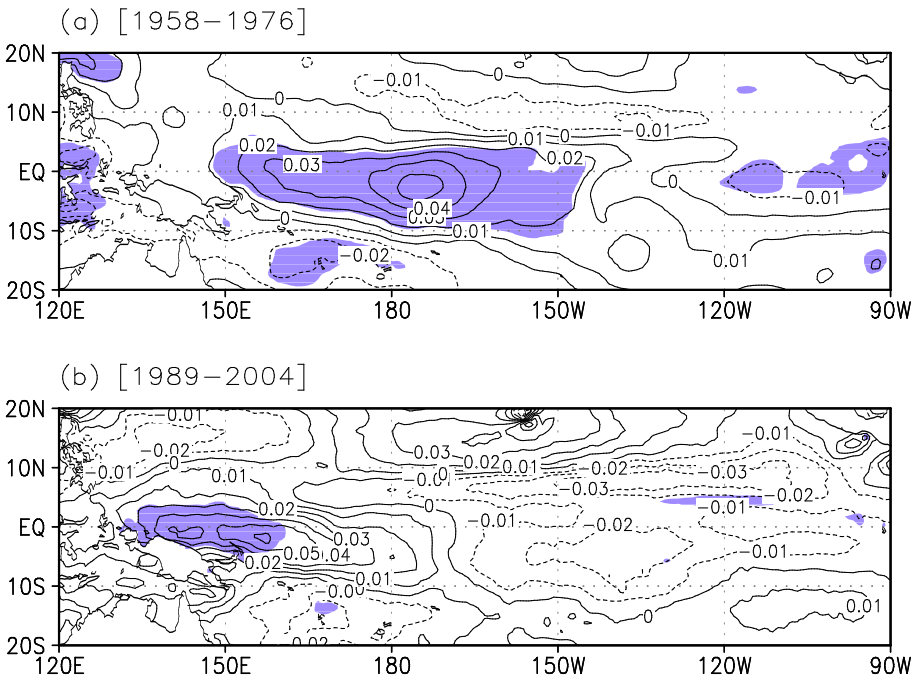

Fig. 4.15. The same as in Fig.4.14 except for zonal wind stress.

Figure 4.16a shows the mean longitude-temperature section along the equator between the W1 and W3 periods, indicating that temperature structures alternate signs in the vertical direction in the western and central equatorial Pacific. Furthermore, the vertical temperature gradient is quite large in the warm pool region (140°E–170°W), where there is also a significant change in vertical stratification as shown in Fig. 4.16b.

Figure 4.16b shows the vertical profile of mean buoyancy frequency, $N^2(z)(=-\frac{g}{\rho}\frac{\partial \rho}{\partial z})$, for the warm pool region (140°E–170°W) along the equator during the two aforementioned sub-periods. The variable N^2 is the Brunt-Väisälä frequency, calculated using SODA data. The vertical profile of mean buoyancy frequency for the eastern tropical Pacific (150°W–90°W) is compared between the two sub-periods and there is little change in vertical stratification. These results support the hypothesis that significant changes in vertical stratification at the upper levels mostly occur in the warm pool region, and that these changes are associated with changes in the warm pool SST. Vertical stratification at relatively shallow depths (100–200 meters) is significantly greater during the W3 period than during the W1 period. Figure 4.16c shows the time series of the maximum value of N^2 averaged over the warm–pool region in 100-200 meters, which represents the intensity of vertical stratification, for 1958–2004. The maximum value of N^2 also gradually increases over time,

and a simultaneous correlation between the time series of the maximum N^2 and the WPI is 0.65, which is statistically significant at the 95% confidence level. Although a correlation coefficient does not imply a cause-effect relationship, a high correlation coefficient may indicate that the changes in the vertical stratification are largely due to the variations in warm pool SST (An *et al*. 2008; Di Nezio *et al*. 2009).

It is noteworthy that the lead-lagged relationship between the two time series indicates that the maximum correlation coefficient is obtained at the zero-lagged time. Furthermore, it is found that the relationship between the maximum N^2 and the WPI is strengthened in the W3 period compared to the W1 period. A simultaneous correlation between the time series of the maximum N^2 and the WPI is 0.71 in the W3 period, which is higher than that in the W1 period, 0.47. Despite the fact that two different datasets were used, the strong correlation observed between maximum $N^2(z)$ and WPI may support that increased stratification is largely due to an increase in warm pool SST. In particular, the variations in the maximum stratification are highly associated with the warm pool SST variations in the W3 period. Because the mean SST in the warm pool region during the W3 period is warmer than that during the W1 period (e.g., Fig. 4.13c), this result may indicate that the variations of warm pool SST under a warm state of SST are more associated with the changes in the vertical

stratification.

On the other hand, one may argue that such vertical stratification change (Fig. 4.16a) might be associated with the variations of thermocline depth. Figure 4.17 shows the time series of thermocline depth averaged over the region [140°E–170°W, 10°S–10°N], which corresponds to the warm pool region. The thermocline depth is defined as the 20℃ isotherm depth in the SODA data. It is evident that the thermocline depth becomes shallower from the W1 period to the W3 period, which is consistent with the temperature structures as shown in Fig. 4.16a. The mean thermocline depth in the two periods is 178.4 m and 165.1 m, respectively. In contrast to the WPI, however, the change in the thermocline depth is distinct before and after the mid-1970s as suggested by previous study (Ashok *et al*. 2007). In spite of this, the changes of stratification intensity are more closely associated with WPI than the variations of thermocline depth. A simultaneous correlation between the time series of the maximum N^2 and the thermocline depth variations is -0.19 for the entire period, indicating there is no significant relationship between the two variabilities. This suggests that the stratification intensity change between the W1 and the W3 periods is mostly associated with the processes at shallower depth in the warm pool above the thermocline depth.

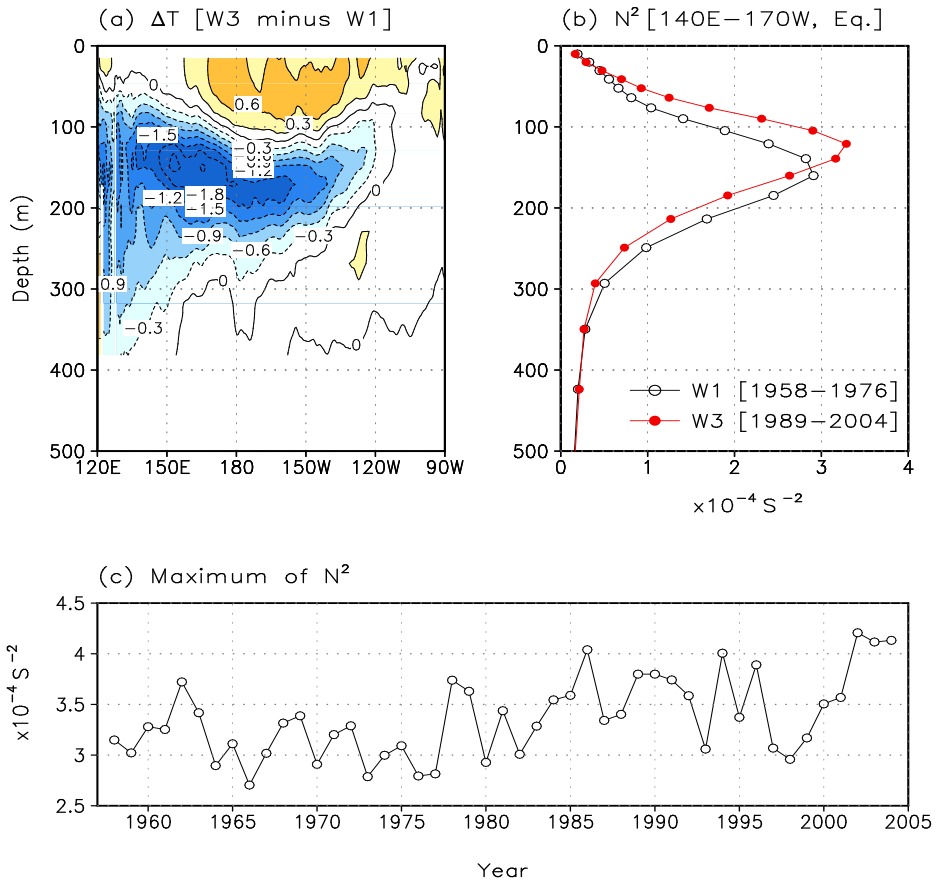

Fig. 4.16. (a) Difference of vertical temperature along the equator between the mean over W3 [1989–2004] and the mean over W1 [1958–76], (b) vertical profiles of the Brunt-Väisällä buoyancy frequency ($N^2(z)$), for the periods W1 [1958–76] (black open circle) and W3 [1989–2004] (red closed circle), and (c) the time series of maximum value of the Brunt-Väisällä buoyancy frequency for the period 1958–2004.

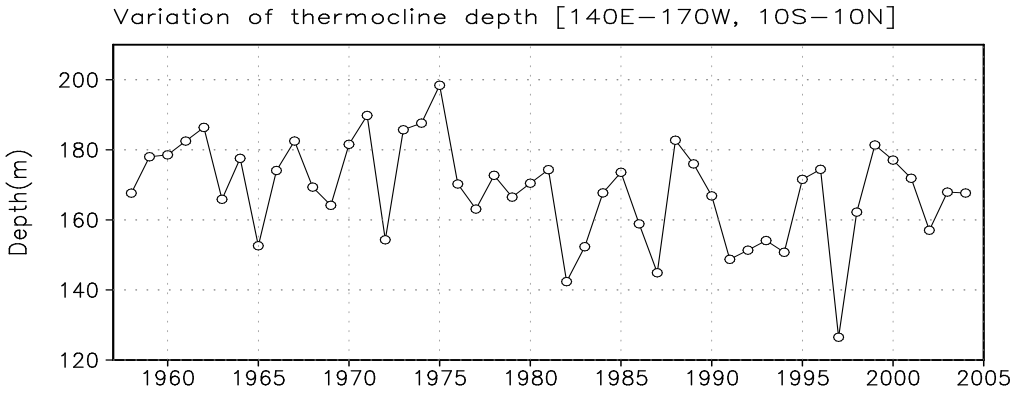

Fig. 4.17. Time series of thermocline depth over the region [140°E–170°W, 10°S–10°N] based on SODA.

4.3.2 Possible linkage between ocean stratification and warm pool SST change

Atmospheric winds drive ocean currents by applying wind stress to the upper oceanic layer. The momentum is then transported vertically into the ocean, which is dependent of the ocean stratification. The different levels of stratification between the W1 and the W3 periods results in a difference in the vertical distribution of atmospheric momentum projection during each of these time periods. Furthermore, changes in vertical stratification are associated with changes in the oceanic baroclinic mode energy distribution, which is associated with fluctuations in the oceanic baroclinic modes (Dewitte *et al*. 2007; Moon *et al*. 2004, 2007). This study analyzes the projection coefficient (P_n) of wind stress on the first three baroclinic modes. The method is described in section 2.2.2.

Before showing the time series of projection coefficient, the changes in the wind stress forcing between the W1 and the W3 periods is displayed. It is found that the zonal wind stress forcing is significantly enhanced from the W1 period to the W3 period as shown in Fig. 4.18a. In particular, the enhanced zonal wind stress forcing between the two periods is significant in the western and central tropical Pacific (150°E–150°W, 5°S–5°N), which mostly covers the warm pool region. Furthermore, one can also find that the zonal wind stress standard deviation gradually increases more than 100% in the western and central

tropical Pacific from the W1 period to the W3 period on the low-frequency timescales as shown in Fig. 4.18b, which is consistent with the result in Fig. 4.18a. Therefore, an enhanced variability of zonal wind stress forcing from the W1 period to the W3 is observed over the warm pool, indicating that the increase of warm pool SST may influence further the atmosphere. It is necessary to explore in more details what is responsible for such enhanced variability of zonal wind stress forcing and in turn how such change in wind stress influences the warm pool SST variability through the changes in the ocean dynamics and heat flux variations. This issue is difficult to tackle with without dedicated model experiments and therefore is beyond the scope of the present study. Rather we focus on how warm pool SST changes relate to the fluctuations of the vertical stratification which is influential on the ocean dynamics.

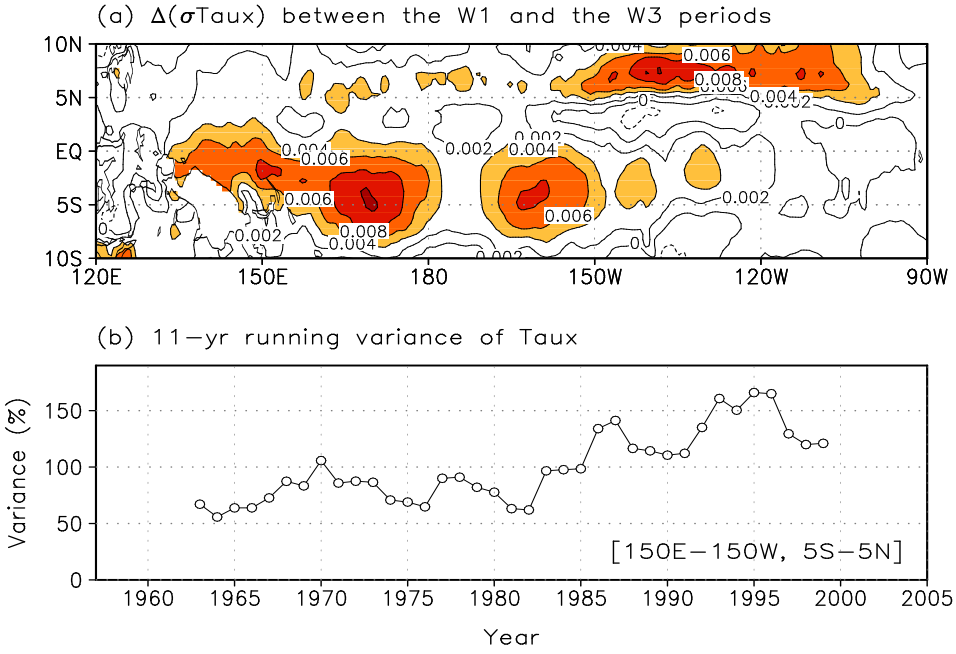

Fig. 4.18. (a) Difference of the standard deviation of zonal wind stress anomalies between the W1 [1958–76] and the W3 [1989–2004] periods, and (b) the percentage of 11-year running variance of the zonal wind stress anomalies over the region [150°E–150°W, 5°S–5°N] for the period 1958–2004 based on the SODA data. Contour interval is 0.002 and unit is N/m^2 in (a), and the standard deviation is normalized by the mean value.

Without doubt, both changes in the SST and atmospheric wind stress forcing may significantly modulate surface momentum flux projecting on the oceanic baroclinic mode in the warm pool, which results in the changes in the projection coefficients. Fig. 4.19 shows the time series of projection coefficients corresponding to the first three baroclinic modes (hereafter, P_1, P_2, and P_3,), averaged over the warm pool region (140°E–170W, 10°S–10°N) for the period 1958–2004. The largest projection coefficient in the warm pool region is P_1, which indicates that wind stress forcing over the warm pool primarily projects onto the first oceanic baroclinic mode compared to the second and third oceanic baroclinic mode. One can find that all of the projection coefficients tend to increase over time, indicating that surface momentum flux projecting onto the first three baroclinic modes is enhanced. Therefore, the equatorial wave dynamics became more effective through the larger projection of the wind stress forcing onto modes 1, 2 and 3, which is consistent with previous studies (Moon *et al*. 2004; Lee *et al*. 2012). An increase rate of P_1 is not large, however, small increase of P_1 from the W1 period to the W3 period is able to change the oceanic baroclinic mode energy distribution projecting onto the first oceanic baroclinic mode between the two periods because wind stress forcing over the warm pool primarily projects onto the first oceanic baroclinic mode as mentioned above. On the other hand, P_2 increases relatively more than P_1 and

P_3. This indicates that there is greater surface momentum flux projecting onto the second baroclinic modes in the warm pool region from W1 period to W3 period. Table 4.3 displays a relationship of the WPI and the thermocline depth variations along with the projection coefficients (P_n, n=1, 2, 3). It is evident that while P_1 is strongly correlated with the WPI, P_2 and P_3 are highly correlated with the thermocline depth variations in the warm pool region for the period 1958–2004. This result indicates that surface momentum flux projecting onto the higher (i.e., second and third) oceanic baroclinic modes is associated with the variations of thermocline depth in the warm pool region, on the other hand, that projecting onto the first baroclinic mode is associated with the SST variations in the warm pool region. Therefore, a shallowing of thermocline depth from the W1 period to the W3 period is associated with the changes of oceanic baroclinic mode energy distribution for the higher-order (i.e., second and third) baroclinic mode fluctuations, which leads to an increase of P_2 and P_3. On the other hand, a warming of warm pool SST, which is associated with changes in vertical stratification, leads an increase of the relationship between P_1 and WPI. It is useful to investigate the P_1 to examine how the warm pool SST influences the tropical Pacific climate system via the variability of oceanic baroclinic modes.

Figure 4.20 display the regressed zonal wind stress to the P_1 for the W1 and W3 period, respectively. First of all, the spatial pattern of regressed zonal wind

stress is quite different between the two sub-periods. Because the wind stress acting on a baroclinic mode depends on the vertical structure function, the results in Fig. 4.20 indicate that the zonal wind stress forcing projecting onto the first baroclinic mode in the warm pool region changes from the W1 period to the W3 period. This is mostly due to changes in vertical stratification as discussed earlier. For the W1 period, the regressed zonal wind stress forcing is large in the central equatorial Pacific and one can find that a center of maximum zonal wind stress forcing is located in the east of dateline. Such structure well represents the zonal wind stress forcing associated with ENSO, in particular the case of ENSO in which the center of its maximum anomalous SST is located in the eastern tropical Pacific.

On the other hand, the regressed zonal wind stress is significant in the western and eastern equatorial Pacific for the W3 period, respectively (Fig. 4.20b). Positive zonal wind stress in the western equatorial Pacific might be associated with an eastward movement of warm water in the warm pool region, in contrast, that in the eastern equatorial Pacific may induce the cooling in the eastern equatorial Pacific via the strengthening of zonal trade winds. Consequently, such wind stress structure is associated with El Niño in which the center of its maximum anomalous SST is located in the central tropical Pacific. Therefore, one may expect that changes in wind stress forcing projecting

onto the first baroclinic mode turns out the changes in the variability of anomalous SST in the tropical Pacific Ocean from the W1 period to the W3 period.

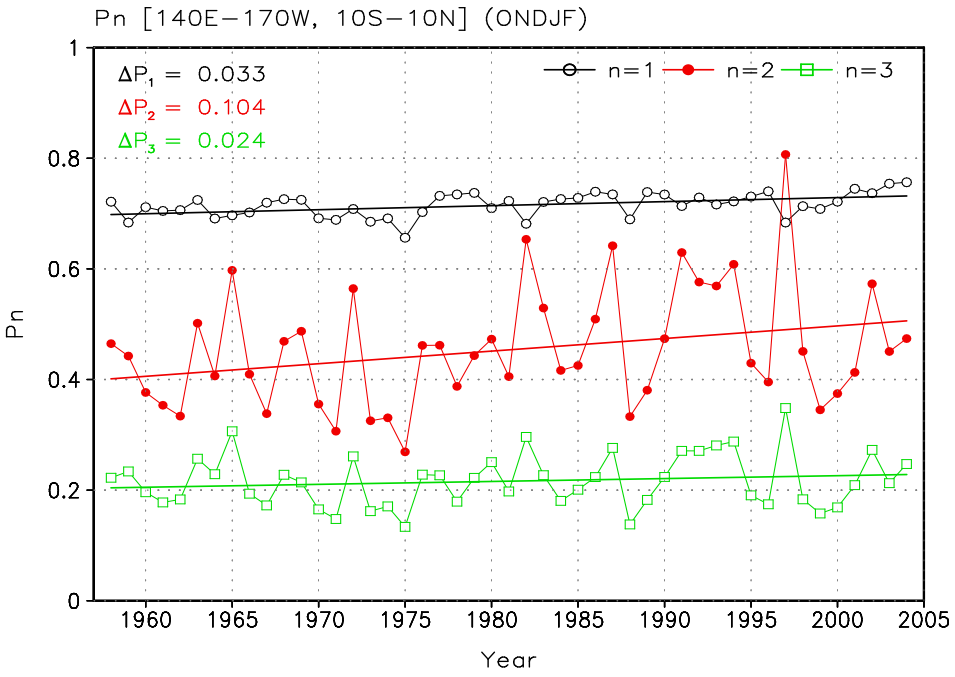

Fig. 4.19. The time series of the first three mean projection coefficients (P_n, n=1, 2, 3) averaged over the region [140°E–170°W, 10°S–10°N] for the period 1958-2004.

Table 4.3. Correlation coefficients between P_n (n=1, 2, 3) and WPI/TDI (1958–2004 and 1989–2004).

		P_1	P_2	P_3
WPI	1958–2004	0.73	0.38	0.33
	1989–2004	0.86	0.36	0.34
TDI	1958–2004	-0.15	-0.95	-0.90
	1989–2004	-0.26	-0.97	-0.89

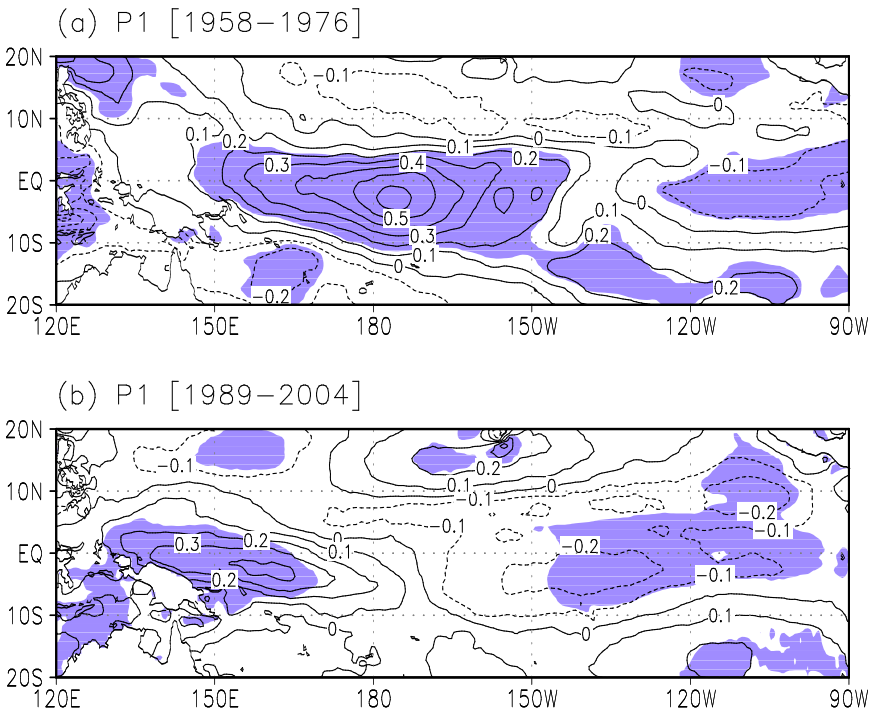

Fig. 4.20. Regressed zonal wind stress against P_1 for the (a) W1 period [1958-1976] and W3 period [1989-2004]. Shaded areas are significant at 95 % confidence level.

The time series of the maximum value of N^2 is also strongly correlated with the time series of P_1 for the period 1958–2004 (r=0.69). Moreover, such correlation is increased from the W1 period (r =0.43) to the W3 period (r =0.73). However, there is little relationship between the time series of the maximum N^2 and the time series of P_2 and P_3 in the warm pool region. This indicates that the variability of P_2 represents the variability of vertical stratification intensity in the warm pool region. Therefore, one may argue that an increase of ocean stratification in the warm pool region is more influential on the variability of the wind stress forcing projecting onto the first oceanic baroclinic mode than any other higher-order baroclinic modes. To illustrate this latter statement, Fig. 4.21 displays the 11-year running mean time series of the root mean square of anomalous zonal wind stress forcing projected onto the first three oceanic baroclinc modes averaged in the warm pool region. Note that the anomalous zonal wind stress forcings projected onto the first three oceanic baroclinic modes (hereafter, P_1 *Taux, P_2 *Taux and P_3 *Taux) are obtained from multiplying the projection coefficients by the anomalous zonal wind stress at each grid point.

It is obvious the magnitude of P_1*Taux in the warm pool region is large compared to that projected onto the high-order baroclinic modes, i.e., P_2*Taux and P_3*Taux. In addition, it is enhanced from the W1 period to the W3 period,

indicating that the variability of zonal wind stress forcing projecting onto the first oceanic baroclinic mode became large and increased stratification favors the enhancement of the variability of zonal wind stress projecting onto the first oceanic baroclinic mode from the W1 period to the W3 period. It is noteworthy that changes for P_2*Taux are as large for P_1*Taux, which is consistent with Moon *et al*. (2004) and Dewitte *et al*. (2009). However, it might be argued that an increase of P_1**Taux was more effective to influence on warm pool SST and baroclinic energy distribution compared to P_2*Taux and P_3*Taux because of its large magnitude in the warm pool region.

Interestingly, it was found that the P_1*Taux was more correlated with the SST variability in the central tropical Pacific (NINO4 region, 160°E–150°W, 5°S–5°N) compared to the eastern tropical Pacific (NINO3 region, 150°W–90°W, 5°S–5°N) as shown in Table 4.4. This result indicates that the variability of P_1*Taux is more influential to the SST variability in the central tropical Pacific compared to the eastern tropical Pacific. Therefore, it is possible that an enhancement of P_1*Taux during recent period can cause an increase of SST variability in the central tropical Pacific compared to that in the eastern tropical Pacific. That is, the anomalous SST variability, which is associated with the first baroclinic oceanic mode, may contribute to change the structure of total anomalous SST in which a center of maximum anomalous SST is shifted to the west for the W3

period.

As mentioned earlier in previous (section 1.1), there are two different types of El Niño; the conventional El Niño and the non-conventional El Niño. Non-conventional El Niño has occurred more frequently during recent decades Changes in the wind stress forcing projecting onto the first baroclinic mode in the warmpool, which are related to changes in vertical stratification, may thus contribute to an increase in the occurrence of non-conventional El Niño during recent decades.

To further examine this argument, the regressed zonal wind stress against with NINO3 SST index for the W1 period, and the El Niño Modoki Index (hereafter, EMI) for the W3 period as shown in Fig.4.22a and b, respectively. The spatial pattern of regressed zonal wind stress against NINO3 SST is similar to regressed zonal wind stress against P_1. This suggests that, for the W1 period, the surface momentum forcing projected onto the first baroclinic mode over the warm pool region tends to contribute to the anomalous SST in the central and eastern tropical Pacific. The EMI represents the variability of non-conventional El Niño (Ashok et al. 2007), is defined as [SSTA]A-0.5*[SSTA]B-0.5[SSTA]C. The square bracket in the equation represents the area-averaged SST anomaly over each of the regions A(165°E–140°W, 1°S–10°N), B(110°W–70°W, 15°S–5°N), and C(125°E–145°E, 10°S20°N), respectively. The structure of regressed SST

anomalies is characterized by the maximum anomalous SST which is located in the central tropical Pacific, which is quite similar to the structure of the non-conventional El Niño as suggested by previous studies (Ashok *et al*. 2007). On the other hand, the zonal wind stress against with the EMI (Fig. 4.22b), which is associated with the non-conventional El Niño, is characterized by the westerlies in the western equatorial Pacific and the easterly in the eastern equatorial Pacific. The westerlies of equatorial central Pacific are also significant, which is in contrast to the regressed zonal wind stress to the NINO3 SST index (Fig. 4.22a). The regressed zonal wind stress anomalies against EMI for the W3 period (Fig. 4.22b) is similar to the regressed zonal wind stress anomalies against P_1 for the W3 period (Fig. 4.20b), and the pattern correlation coefficient is 0.56. This indicates that the surface wind stress forcing projecting onto the first baroclinic mode contributes to the wind stress forcing which may lead to the non-conventional El Niño after the late-1980s.

Fig. 4.23 shows the regressed anomalous SST (shade) and wind (vector) against P_1 for the W1 period and W3 period. Basically, the regressed anomalous SST against with the P_1 is quite different between the two periods. This result indicates that the anomalous SST responding to the wind stress forcing projecting onto the first baroclinic oceanic mode is different between the two periods, which is associated with the changes in the oceanic vertical

stratification. The anomalous SST, which is associated with the amount of wind stress forcing projecting onto the first baroclinic mode for the W1 period, is characterized by the variability in a basin-like structure along with a center of maximum in the central and eastern tropical Pacific. In contrast, the anomalous SST, which is associated with the amount of wind stress forcing projecting onto the first baroclinic mode for the W3 period, is characterized by an east-west contrasting structure in the tropical Pacific basin. That is, the anomalous SST, which is associated with the first baroclinic oceanic mode, may contribute to change the structure of total anomalous SST in which a center of maximum anomalous warm (cool) SST is shifted to the west in an El Niño (La Niña) event for the W3 period. During the W1 period, wind convergence is located in the central and eastern tropical Pacific. In contrast, during the W3 period, and wind convergence is also shifted westward around the date-line.

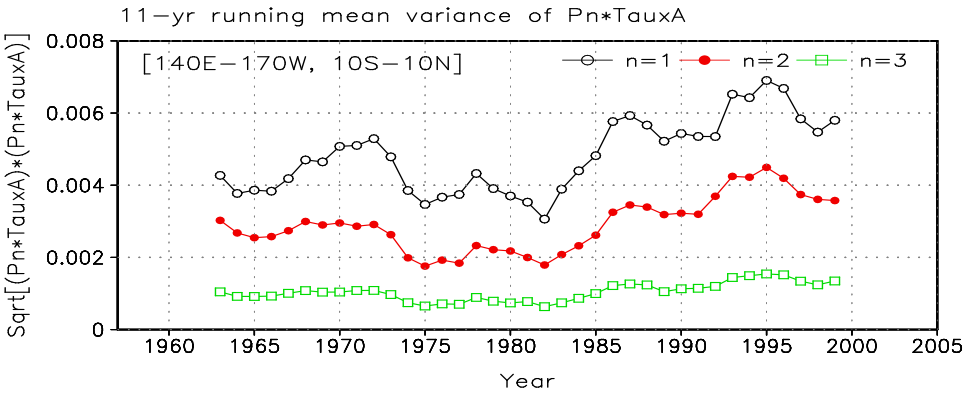

Fig. 4.21. 11-yr running mean of the root mean square of the zonal wind stress anomalies for the contribution of the first three oceanic baroclinic modes (i.e., P_1*Taux, P_2*Taux and P_3*Taux) over the region [140°E–170°W, 10°S–10°N] for the period 1958–2004.

Table 4.4. Correlation coefficients between P_1*Taux and the NINO3 & NINO4 SST index during period 1958–2004.

	P_1*Taux
NINO3 SST index	0.53
NINO4 SST index	0.73

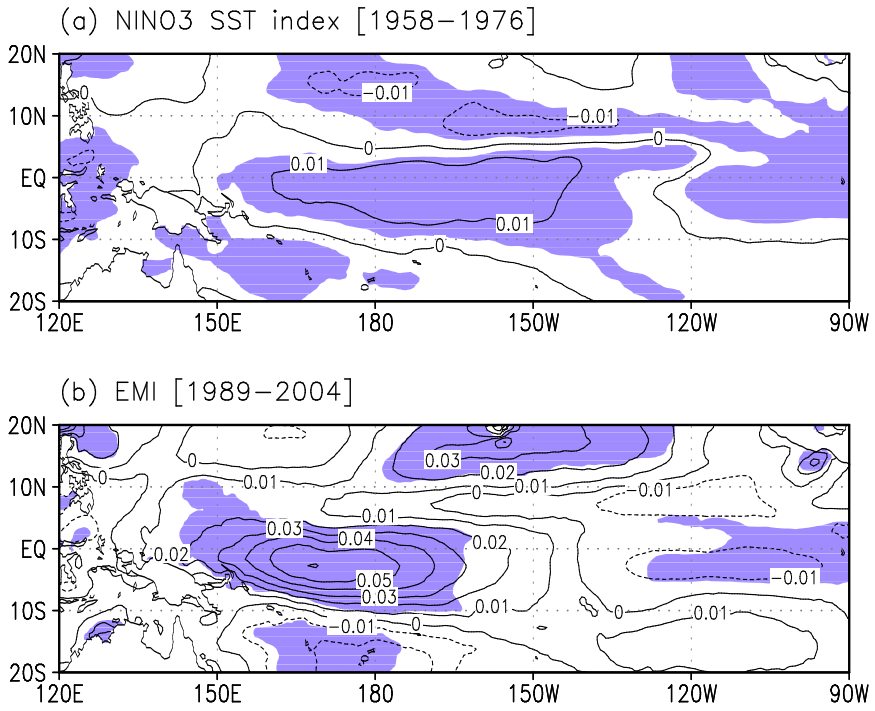

Fig. 4.22. The same as in Fig.4.20 except for (a) NINO3 SST index for the W1 period (1958-1976) and (b) El Niño Modoki index (EMI) for the W3 period (1989-2004). EMI is defined as [SSTA]A-0.5*[SSTA]B-0.5[SSTA]. The square bracket in the equation represents the area-averaged SST anomaly over each of the regions A(165°E–140°W, 10°S–10°N), B(110°W–70°W, 15°S–5°N), and C(125°E–145°E, 10°S–20°N).

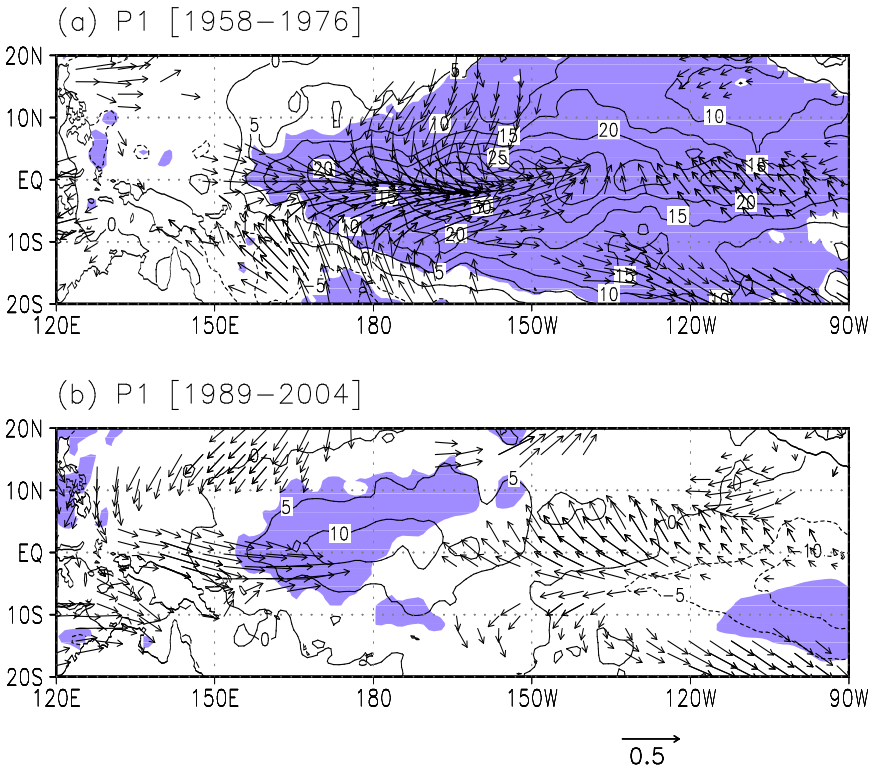

Fig. 4.23. Regressed sea surface temperature (contour) and wind stress (vector) against the P_1. Shaded areas are significant at 95 % confidence level.

At this stage, it is useful to check how changes in P_1*taux documented above project onto the zonal circulation in the equatorial Pacific. Figure 4.24 shows the correlation between the surface zonal currents over the warm pool region and sea surface temperature anomalies. The correlation increased over the warm pool region in the first three modes from the W1 period to W3 period. The first baroclinic mode has the largest variation in the warm pool region. It means that the change in stratification impacts the zonal circulation onto the first baroclinc mode. Fig. 4.25 shows the root mean square of surface zonal current anomalies for the contribution of the first three baroclinic modes during the W1 period (Figs. 4.25a–c) and the W3 period (Figs. 4.25d–f). Figures 4.25g–i are the difference of root mean square between the two periods. Larger values for zonal current variance are confined within 5°S–5°N during the two periods. For mode 1, maximum variance is centered in the western equatorial Pacific, whereas the contribution of the second and third baroclinic mode is important in the eastern equatorial Pacific. It is evident that the contribution for the first baroclinic mode increases in the western and central equatorial Pacific (Fig. 4.25g) where the variability of zonal wind stress forcing is enhanced from the W1 period to the W3 period (Fig. 4.25). The first mode enhanced the westward currents while the second and the third mode enhanced the eastward currents. This suggests a reduction (an increase) of the zonal current variability (locally wind–driven

current) in the western-central (eastern) Pacific. It tends to indicate that the increase of wind stress variability in the central–western Pacific will project more on the baroclinic component of the current.

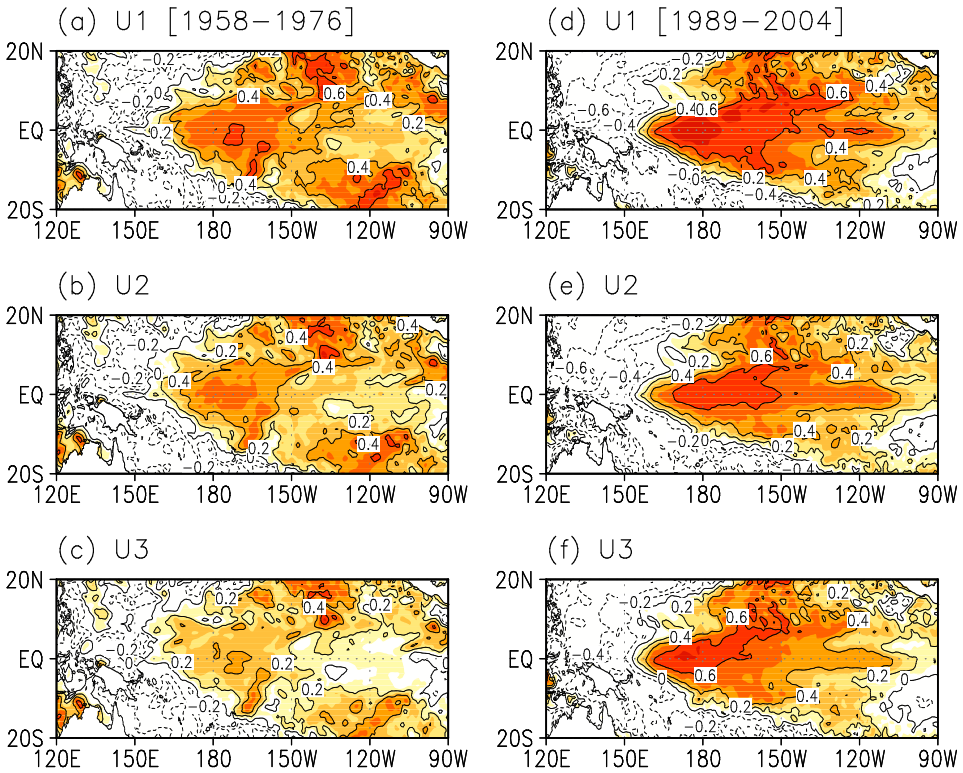

Fig. 4.24. Correlation map between surface zonal currents averaged over the warm pool region for the contribution of (a) the first mode, (b) the second mode, and (c) the third mode and sea surface temperature for the W1 period [1958-1976]. (d)–(f) is the same as in (a)–(c) except for the W3 period [1989–2004].

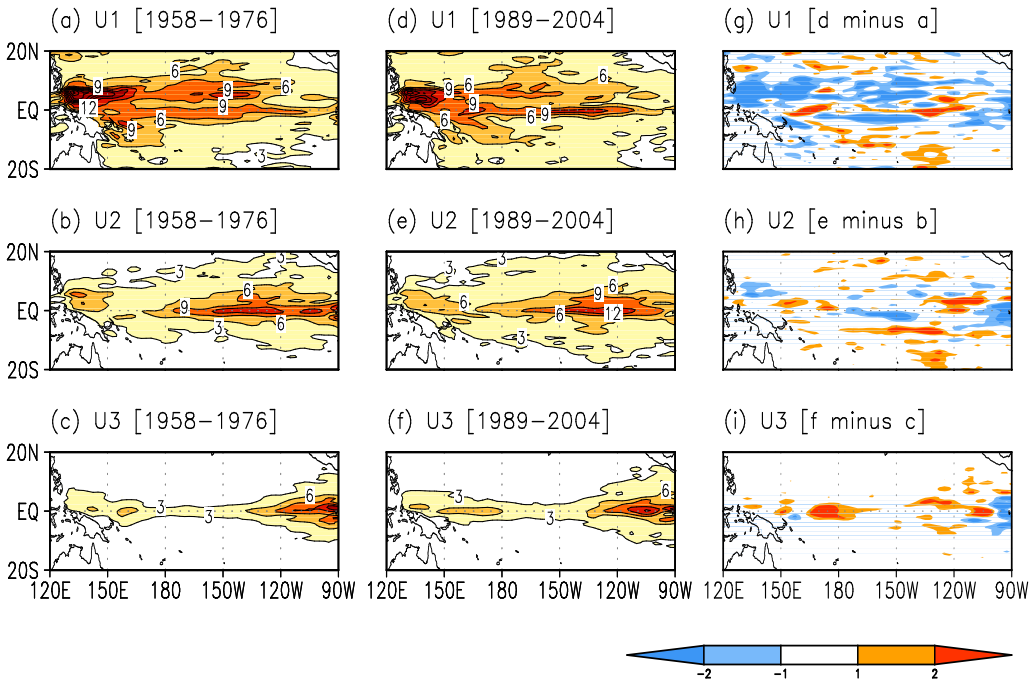

Fig. 4.25. The root mean square of surface zonal currents for the contribution of (a) the first mode, (b) the second mode and (c) the third mode for the W1 period [1958-1976]. (d)–(f) is the same as in (a)–(c) except for the W3 period [1989–2004]. Units are cm s^{-1} and contour intervals are every cm s^{-1}. (g)–(i) are the difference of rms between the two periods ((d)–(f) minus (a)–(c)).

CHAPTER 5

CONCLUSION

This dissertation focuses on the characteristics of surface wind stress and ocean stratification variability and their role on the decadal changes in El Niño-Southern Oscillation. There was a significant change in period and intensity of ENSO before and after the late-1970s.

The cause of the change of ENSO period and intensity is explained by wind stress change in the western Pacific. The positive wind stress curl was generated before ENSO mature state and stronger before the late-1970s than that after the late-1970s. On the other hand, the wind stress curl is relatively weak before the late-1970s, make the period and intensity of ENSO become longer and stronger, respectively, by slowing discharge of heat content within the thermocline depth.

The observational results are verified by simple coupled model experiments. In the numerical experiment, the period of ENSO is 5 year in the CTL experiment and 3.5 year in the WNP experiment, respectively. This shows that the wind stress change proportional the change of the zonal-mean thermocline depth that make the short period and weak intensity of ENSO.

The wind stress forcing has decadal change and the first and second baroclinic mode increases after the late–1970s. The maximum standard deviation is located in the central Pacific. The maximum correlation coefficient between the NINO3 SST index and zonal wind stress forcing is also presented in the central Pacific. The interannual variability in wind stress projection coefficient of the first three baroclinic modes experiences significant changes around before and after the late–1970s. These changes reflect changes in ENSO feedback processes because each mode has a specific effect on the coupled instabilities of the tropical Pacific system through their meridional scale of variability (i.e., the higher the order of baroclinic mode, the finer the meridional scale), propagation characteristics and contribution to the momentum flux. Whereas most studies have focused on the changes in stratification on longer timescales (Moon *et al*. 2004; Dewitte *et al*. 2007), the inspection of these changes on interannual timescales and their relation with ENSO offer an alternative view for interpreting changes in ENSO properties on decadal timescales. In

particular, it allows estimating the coupling efficiency associated with each baroclinic mode in the development of ENSO. The first three baroclinic modes were selected here because of their propagating characteristic and significant contribution to ENSO variability (Dewitte *et al*. 1999). The summed-up contribution of the higher-order modes, although trapped within the mixed layer, can also have a significant contribution to the interannual variability in the tropical Pacific (Dewitte *et al*. 1999). In particular, if the wind stress forcing onto the high-order baroclinic modes were weakened after the late-1970s, the author may argue that changes in the equatorial wave dynamics, associated with the variability of the first three oceanic baroclinic modes, is a key process involved in the change in the ENSO variability after the late-1970s.

EOF analysis was performed to examine the warm pool SST variability. The spatial variance of the SST shows warming (increasing) trend over the warm-pool (cooling in the eastern Pacific and warming in the western Pacific). The warm pool index (WPI) has positive correlation with SST EOF PC1 (or PC2). Through the EOF analysis, this dissertation links the SST variability in the warm pool to the changes in the tropical Pacific mean-state and the ENSO characteristics. It was found that the leading mode of warm pool SST variability reflected the shift of the Pacific mean state toward a La Niña-like condition. This mean state change is consistent with that suggest by the ocean thermostat

theory.

It was discussed how the mean SST changes to a La Niña-like pattern, which is associated with the EOF1 of the warm pool SST anomaly, is related with a frequent occurrence of the CP El Niño. That is, the enhanced zonal mean SST gradient in the central equatorial Pacific, due to the mean SST changes toward a La Niña-like pattern, is able to lead to the CP El Niño through the enhancement of the zonal advective feedback processes. Furthermore, we examined how these two modes of SST variability are associated with the vertical structure in the ocean temperature. It is found that the EOF1 and EOF2 have large differences in their associated subsurface temperature structures along with the structure of thermocline depth. The EOF1 mode of warm pool SST variability is accompanied with an increased sloping of the thermocline depth in the equatorial Pacific. In contrast, the EOF2 of warm pool SST variability is associated with an east-west flattening of thermocline depth.

The warming of warm pool SST influences tropical Pacific SST variability through changes in oceanic baroclinic mode characteristics. Based on the time series of SST anomalies averaged over the warm pool region (WPI), the warm pool SST is characterized by cooling and warming in sub-periods 1958–76 (W1 period) and 1989–2004 (W3 period), respectively. Comparing these two sub-periods shows that changes in the warm pool SST influence tropical Pacific

SST variability via the variability of oceanic baroclinic modes.

Changes in warm pool SST are associated with changes in vertical stratification of the warm pool region. Vertical stratification substantially increases at the upper layers from the W1 period to the W3 period. In particular, the maximum value of mean buoyancy frequency for the warm pool region gradually increases and is significantly correlated with warm pool SST variability rather than the variations of thermocline depth, supporting the hypothesis that increased stratification is largely due to an increase of warm pool SST. Further analysis shows that from the W1 period to the W3 period there are significant changes in temperature structures at shallower depths in the tropical Pacific, which are largely associated with the enhanced stratification in the warm pool region compared to the eastern tropical Pacific. In addition, the variability of zonal wind stress forcing over the warm pool region is also significantly enhanced form the W1 period to W3 period.

Projection coefficients of wind stress onto the first three baroclinic modes were used to examine the influence of vertical stratification in the warm pool region. P_n (n=1, 2, 3) tends to increase over time. Because P_1 is dominant over the warm pool, therefore, it may be the best predictor of vertical stratification in the region. That is, variations of P_1 are closely associated with warm pool SST change, which in turn are related with changes in vertical

stratification. In other words, an increase of ocean stratification in the warm pool region is more influential on the variability of the wind stress forcing projecting onto the first oceanic baroclinic mode than any other higher-order baroclinic modes. To illustrate this, it was calculated the root mean square of anomalous zonal wind stress forcing projected onto the first three oceanic baroclinc modes averaged in the warm pool region (i.e., P_1*Taux, P_2*Taux and P_3*Taux). It is found that the magnitude of P_1*Taux in the warm pool region is enhanced from the W1 period to the W3 period, indicating that the variability of zonal wind stress forcing projecting onto the first oceanic baroclinic mode becomes large.

Our further analysis indicates that the P_1*Taux is highly correlated with the SST variability in the central tropical Pacific compared to the eastern tropical Pacific. Therefore, an enhancement of P_1*Taux during recent period can cause an increase of SST variability in the central tropical Pacific compared to that in the eastern tropical Pacific. Similarly, it is found that the contribution of the first baroclinic mode on the surface zonal current anomalies increases in the western and central equatorial Pacific where the variability of zonal wind stress forcing is enhanced from the W1 period to the W3 period. The author argue that changes in the wind stress forcing projecting onto the first baroclinic mode in the warm pool, which are related to changes in vertical

stratification, may thus contribute to an increase in the occurrence of non-conventional El Niños during recent decades.

REFERENCES

An, S.-I., and B. Wang, 2000: Interdecadal change of the structure of the ENSO mode and its impact on the ENSO frequency. *J. Climate*, **13**, 2044-2055.

An, S.-I., and I.-S. Kang, 2001: Tropical Pacific basin-wide adjustment and oceanic waves. *Geophys. Res. Lett*., **28**, 3975-3978.

An, S.-I, J.-S. Kug, Y.-G. Ham, I.-S. Kang, 2008: Successive Modulation of ENSO to the Future Greenhouse Warming. *J. Climate*, **21**(1), 3-21. doi:10.1175/2007JCLI1500.1

An, S.-I., J.-W. Kim, S.-H. Im, B.-M. Kim, J.-H. Kim, 2012: Recent and future sea surface temperature trends in tropical Pacific warm pool and cold tongue regions. *Climate Dyn*., **39**(6), 1373-1383. DOI: 10.1007/s00382-011-1129-7.

Ashok, K., S. K. Behera, S. A. Rao, H. Weng, and T. Yamagata, 2007: El Niño Modoki and its possible teleconnection. *J. Geophys. Res*., **112**(C11), C11007. doi: 10.1029/2006jc003798

Bjerknes, J., 1969: Atmospheric teleconnections from the equatorial Pacific. *Mon. Wea. Rev*., **97**, 163-172.

Cane, M. A., 1984: Modeling sea level during El Niño. *J. Phys. Oceanogr*., **14**, 1864-1874.

Cane, M. A., A. C. Clement, A. Kaplan, Y. Kushnir, D. Pozdnyakov, R. Seager, S. E. Zebiak, R. Murtugudde, 1997: Twentieth-Century Sea Surface Temperature Trends. *Science*, **275**(5302), 957-960. 10.1126/science.275.5302.957

Carton, J. A., and B. Giese, 2008: A reanalysis of ocean climate using Simple Ocean Data Assimilation (SODA). *Mon. Wea. Rev*., **136**, 2999-3017.

Carton, J. A., G. Chepurin, X. Cao, and B. Giese, 2000: A Simple Ocean Data Assimilation Analysis of the Global Upper Ocean 1950–95. Part I: Methodology, *J. Phys. Oceanogr*., **30**, 294-309.

Carton J. A., G. Chepurin, X. Cao, 2000: A Simple Ocean Data Assimilation Analysis of the Global Upper Ocean 1950–95. Part II: Results, *J. Phys. Oceanogr.* **30**(2),311-326. doi:10.1175/1520-0485(2000)030<0311:ASODAA>2.0.CO;2

Clement, A. C., R. Seager, M. A. Cane, and S. E. Zebiak, 1996: An Ocean Dynamical Thermostat. *J. Climate*, **9**, 2190-2196.

Clement A. C., R. Seager, and R. Murtugudde, 2005: Why are there tropical warm pools? *J. Climate*, **1**8, 5294–5311.

Collins, M., 2000: Understanding uncertainties in the response of ENSO to greenhouse warming, *Geophys. Res. Lett.*, **27**(21), 3509-3512.

Collins, M. *et al*, 2005: El Niño- or La Niña-like climate change?. *Clim. Dyn*. **24**(1), 89-104. doi: 10.1007/s00382-004-0478-x.

Collins, M. *et al*, 2010: The impact of global warming on the tropical Pacific ocean and El Niño. *Nat. Geosci*., **3**(6), 391-397. doi:10.1038/NGEO868.

Conkright, M. E. *et al*, 2002: World Ocean Database 2001, vol. 1, Introduction, NOAA Atlas NESDIS, Vol 42, edited by S Levitus, 159 pp, Govt Print Off Washington D.C.

Cravatte, S., T. Delcroix, D. Zhang, M. McPhaden, L. Leloup, 2009: Observed freshening and warming of the western Pacific Warm Pool. *Clim. Dyn*., **33**, 565-589. DOI: 10.1007/s00382-009-0526-7.

De Garidel-Thoron T, Y. Rosenthal, F. Bassinot, L. Beaufort, 2005: Stable sea surface temperatures in the western Pacific warm pool over the past 1.75 million years. *Nature*, **433**(7023), 294-298. doi:10.1038/nature03189.

Dewitte, B., 2000: Sensitivity of an intermediate ocean-atmosphere coupled model of the tropical Pacific to its oceanic vertical structure. *J. Climate*,

13(13), 2363-2388.

Dewitte, B., G. Reverdin, C. Maes, 1999: Vertical structure of an OGCM simulation of the equatorial Pacific Ocean in 1985-94. *J. Phys. Oceanogr.*, 29(7), 1542-1570.

Dewitte, B., S. Thual, S.-W. Yeh, S.-I. An, B.-K. Moon, and B. S. Giese, 2009: Low-Frequency Variability of Temperature in the Vicinity of the Equatorial Pacific Thermocline in SODA: Role of Equatorial Wave Dynamics and ENSO Asymmetry. *J. Climate*, 22, 5783-5795.

Dewitte, B., S.-W. Yeh, C. Cibot, L. Terray, 2007: Rectification of ENSO variability by interdecadal changes in the equatorial background mean state in a CGCM simulation. *J. Climate*, 20(10), 2002-2021. doi: 10.1175/JCLI4110.1.

DiNezio, P. N., A. C. Clement, G. A. Vecchi, B. J, Soden, B. P. Kirtman, and S.-K. Lee, 2009: Climate response of the equatorial Pacific to global warming. *J. Climate*, **22**, 4873-4892.

DiNezio, P. N., A. C. Clement, and G. A. Vecchi, 2010: Reconciling Differencing Views of Tropical Pacific Climate Change. *EOS, Trans. Amer. Geophys. Union*, *91*(16), 141-152.

Eriksen, C. C., 1988: On Wind Forcing and Observed Oceanic Wave Number

Spectra, *J. Geophys. Res*., 93(C5), 4985–4992.

Fedorov, A. V., and S. G. Philander, 2000: Is El Niño Changing?. *Science*, **288**(5473), 1997-2002. doi:10.1126/science.288.5473.1997.

Fu, R., A. D. Del Genio, and W. B. Rossow, 1994: Influence of Ocean Surface Conditions on Atmospheric Vertical Thermodynamic Structure and Deep Convection. *J. Climate*, **7**(7), 1092-1108. doi:10.1175/1520-0442(1994)007 <1092:IOOSCO> 2.0.CO;2.

Giese, B. S., S. C. Urizar, and N. S. Fukar, 2002: Southern Hemisphere origins of the 1976 climate shift. *Geophys. Res. Lett*., **29**, 1–4.

Graham, N. E., 1994: Decadal-scale climate variability in the tropical and North Pacific during the 1970s and 1980s: observations and model results. *Climate Dyn*., **10**, 135-162.

Gu D., and S. G. H. Philander, 1997: Interdecadal climate fluctuations that depend on exchanges between the tropics and extratropics. *Science*, **275**, 805–807.

Guilderson, T. P., and D. P. Schrag, 1998: Abrupt shift in subsurface temperatures in the eastern tropical pacific associated with recent changes in El Niño. *Science*, **281**, 240–243.

Guilyardi, E., 2006, El Niño-mean state-seasonal cycle interactions in a multi-

model ensemble. *Clim. Dyn*., **26**,329-348, DOI: 10.1007/s00382-005-0084-6.

Jin, F.-F., 1996: Tropical ocean-atmosphere interaction, the pacific cold tongue, and the El Niño Southern Oscillation, *Science*, **274**, 76-78.

Jin, F.-F., 1997, An equatorial ocean recharge paradigm for ENSO. Part I: Conceptual model, *J. Atm. Soc.*, **54**, 811-829.

Kang, I.-S., and K.-M. Lau, 1994: Principal modes of atmospheric circulation anomalies associated with global angular momentum fluctuations, *J. Atm. Soc.*, **51**, 1194-1205.

Kang, I.-S., and J.-S. Kug, 2000: An El-Nino prediction System with an intermediate ocean and statistical atmosphere. *Geophys. Res. Lett*., **27**, 1167-1170.

Kang, I.-S., and J.-S. Kug, 2002: El Niño and La Niña SST anomalies: Asymmetry characteristics associated with their wind stress anomalies, *J. Geophy. Rea.*, **107**(D19), 4372, doi10, 1029/2001JD000393.

Kang, I.-S., and S.-I. An, 1998: Kelvin and Rossby wave contributions to the SST oscillation of ENSO, *J. Climate*, **11**, 2461-2469.

Kao, H.-Y., and J.-Y. Yu, 2009: Contrasting Eastern-Pacific and Central-Pacific Types of ENSO. *J. Climate*, **22**(3), 615-632.

Karnauskas, K. B., R. Seager, A. Kaplan, Y. Kushnir, and M. A. Cane, 2009: Observed Strengthening of the Zonal Sea Surface Temperature Gradient across the Equatorial Pacific Ocean. *J. Climate*, **22**, 4316-4321.

Kim, B.-M., and S.-I. An, 2011: Understanding ENSO Regime Behavior upon an Increase in the Warm pool Temperature Using a Simple ENSO Model. *J. Climate*, **24**(5), 1438-1450. doi: 10.1175/2010JCLI3635.1.

Kirtman B. P., 1997: Oceanic Rossby wave dynamics and the ENSO period in a coupled model. *J. Climate*, **10**: 1690-1704.

Knutson, T. R., S. Manabe, D. Gu, 1997: Simulated ENSO in a global coupled ocean–atmosphere model: Multidecadal amplitude modulation and CO_2 sensitivity. *J. Climate*, **10**(1), 138–161.

Kug, J.-S., F.-F. Jin, and S.-I. An, 2009: Two Types of El Niño Events: Cold Tongue El Niño and Warm Pool El Niño. *J. Climate*, **22**(6), 1499-1515. doi:10.1175 2008JCLI2624.1.

Larkin, N. K., and D. E. Harrison, 2005a: On the definition of El Niño and associated seasonal average U.S. weather anomalies. *Geophys. Res. Lett.*, **32**, L13705, doi:10.1029/2005GL022738.

Larkin, N. K., and D. E. Harrison, 2005b: Global seasonal temperature and precipitation anomalies during El Niño autumn and winter. *Geophys.*

Res. Lett., **32**, L16705. doi: 10.1029/2005GL022860.

Latif, M., and T. P. Barnett, 1994: Causes of decadal climate variability over the North Pacific and North America sector, *Science*, **266**, 634-637.

Lee, T., and M. J. McPhaden, 2010: Increasing intensity of El Niño in the central-equatorial Pacific. *Geophys. Res. Lett.*, **37**(14), L14603, doi:10.1029/2010GL044007.

Lee, Y.-K., S.-W. Yeh, B. Dewitte, B.-K. Moon, and J.-G. Jhun, 2012: The influences of interannual stratification variability and wind stress forcing on ENSO before and after the 1976 climate shift. *Theor. Appl. Climatol.*, **107**, 623-631.

Lighthill, M. J., 1969: Dynamical response of the Indian Ocean to onset of the southwest monsoon. *Phil. Trans. R. Soc. A.*, **265**, 45-92, doi: 10.1098/rsta.1969.0040.

Livezey, R. E., and W. Y. Chen, 1983: Statistical Field Significance and its Determination by Monte Carlo Techniques. *Mon. Wea. Rev.*, **111**, 46-59, 10.1175/1520-0493(1983)111<0046:SFSAID>2.0.CO;2

Luo J.-J., and T. Yamagata, 2001: Long-term El Niño-Southern Oscillation (ENSO)-like variation with special emphasis on the South Pacific. *J. Geophys. Res.*, **106**, 22211–22227.

Luo, J. J., S. Masson, S. Behera, P. Delecluse, S. Gualdi, A. Navarra, T. Yamagata, 2003: South Pacific origin of the decadal ENSO-like variations as simulated by a coupled GCM. *Geophys. Res. Lett*., **30**(24), 2250, doi:10.1029/2003GL018649.

McPhaden, M. J., T. Lee, and D. McClurg, 2011: El Niño and its relationship to changing background conditions in the tropical Pacific Ocean. *Geophys. Res. Lett*., **38**, L15709, doi: 10.1029/2011GL048275.

Moon, B.-K., S.-W. Yeh, B. Dewitte, J.-G. Jhun, I.-S. Kang, and B. P. Kirtman, 2004: Vertical structure variability in the equatorial Pacific before and after the Pacific climate shift of the 1970s. *Geophys. Res. Lett*., **31**, L03203, doi:10.1029/2003GL 018829.

Moon, B.-K, S.-W. Yeh, B. Dewitte, J.-G. Jhun, and I.-S. Kang, 2007: Source of low frequency modulation of ENSO amplitude in a CGCM. *Climate Dyn*., 29(1), 101-111. doi:10.1007/s00382-006-0219-4.

Nitta, T., S. Yamada, 1989: Recent warming of tropical sea surface temperature and its relationship to the Northern Hemisphere circulation. *J. Meteor. Soc. Japan*, **67**, 375–383.

North, G. R., T. L. Bell, R. F. Cahalan, and F. J. Moeng, 1982: Sampling Errors in the Estimation of Empirical Orthogonal Functions. *Mon. Wea. Rev*., **110**,

699-706.

Picaut, J., M. Ioualalen, C. Menkes, T. Delcroix, and M. J. McPhaden, 1996: Mechanism of the Zonal Displacements of the Pacific Warm Pool: Implications for ENSO. *Science*, **274**(5292), 1486-1489, doi:10.1126/science. 274.5292.1486.

Pierce, D. W., T. P. Barnett, and M. Latif, 2000: Connections between the Pacific Ocean tropics and midlatitudes on decadal timescales. *J. Climate*, **13**, 1173–1194.

Pierrehumbert, R. T, 1995: Thermostats, Radiator Fins, and the Local Runaway Greenhouse. *J. Atmos. Sci*., *52*(10), 1784-1806, 10.1175/1520-0469(1995)052< 1784: RFATL>2.0.CO;2

Pryce, J. D., 1993: Numerical Solution of Sturm-Liouville Problems. *Oxford University Press*, **322p**.

Ramanathan, V., B. Subasilar, G. J. Zhang, W. Conant, R. D. Cess, J. T. Kiehl, H. Grassl, and L. Shi, 1995: Warm Pool Heat-Budget and Shortwave Cloud Forcing - a Missing Physics. Science, 267(5197), 499-503, doi: 10.1126/ science.267. 5197.499

Rayner, N. A., D. E. Parker, E. B. Horton, C. K. Folland, L. V. Alexander, D. P. Rowel, E. C. Kent, and A. Kaplan, 2003: Global analyses of sea surface

temperature, sea ice, and night marine air temperature since the late nineteenth century. *J. Geophys. Res.*, **108**(D14), 4407, doi:10.1029/2002JD002670.

Rodgers, K. B., P. Friederichs, and M. Latif, 2004: Tropical Pacific decadal variability and its relation to decadal modulation of ENSO. *J. Climate*, 17, 3761–3774.

Seager, R., and R. Murtugudde, 1997: Ocean Dynamics, Thermocline Adjustment, and Regulation of Tropical SST. *J. Climate*, *10*, 521-534.

Sun, D. Z., 1997: El Niño: A coupled response to radiative heating?. *Geophys. Res. Lett.*, **24**(16), 2031-2034, doi:10.1029/97GL01960.

Sun, D. Z., 2003: A Possible Effect of an Increase in the Warm pool SST on the Magnitude of El Niño Warming. *J. Climate*, **16**, 185-205.

Sun, D. Z, and Z. Liu, 1996: Dynamic Ocean-Atmosphere Coupling: A Thermostat for the Tropics. *Science*, **272**(5265), 1148-1150.

Timmermann, A., 2003: Decadal ENSO amplitude modulations: A nonlinear paradigm. *Global Planet. Change*, **37**, 135–156.

Timmermann, A., and F.-F. Jin, 2002: A nonlinear mechanism for decadal El Niño amplitude changes. *Geophys. Res. Lett.*, **2**9, 1003, doi:10.1029/2001GL013369.

Timmermann, A., J. Oberhuber, A. Bacher, M. Esch, M. Latif, and E. Roeckner, 1999. Increased El Niño frequency in a climate model forced by future greenhouse warming. *Nature*, **398**, 694-696.

Trenberth, K. E., and J. W. Hurrell, 1994: Decadal atmosphere-ocean variations in the Pacific, *Climate Dyn.*, *9*, 303-319.

Uppala, S. M. *et al.*, 2005: The ERA-40 re-analysis. *Q. J. R. Meteorol. Soc.*, **131**(612), 2961–3012, doi: 10.1256/qj.04.176.

Vecchi, G.A., and B.J. Soden, 2007: Global Warming and the Weakening of the Tropical Circulation. *J. Climate*, **20**, 4316-4340.

Vecchi, G.A., B.J. Soden, A. T. Wittenberg, I. M. Held, A. Leetmaa, and M. J. Harrison, 2006: Weakening of tropical Pacific atmospheric circulation due to anthropogenic forcing. *Nature*, **441**, 73-76.

Visser, K., R. Thunell, and L. Stott, 2003: Magnitude and timing of temperature change in the Indo-Pacific warm pool during deglaciation. *Nature*, **421**(6919), 152-155, doi:10.1038/nature01297.

Wang, B., R. Wu, and R. Lukas, 1999: Roles of the western North Pacific wind variation in thermocline adjustment and ENSO phase transition *J. Meteor. Soc. Japan*, **77**, 1-16.

Wang, B., and S.-I. An, 2001: Why the properties of El Niño changed during the

late 1970s. *Geophys. Res. Lett.*, **28**, 3709–3712.

Wang, H., and V. M. Mehta, 2008: Decadal Variability of the Indo-Pacific Warm Pool and Its Association with Atmospheric and Oceanic Variability in the NCEP–NCAR and SODA Reanalyses. *J. Climate*, **21**, 5545-5565, doi:10.1175/ 2008JCLI2049.1.

Woodruff, S. D., H. F. Diaz, J. D. Elms, and S. J. Worley, 1998: COADS Release 2 data and metadata enhancements for improvements of marine surface flux fields. *Phys. Chem. Earth*, **23**, 517-526.

Wu, R. and S. P. Xie, 2003: On equatorial Pacific surface wind changes around 1977: NCEP–NCAR reanalysis versus COADS observation. *J. Climate*, **16**, 167–173

Yeh, S.-W., B. Dewitte, J.-G. Jhun, and I.-S. Kang, 2001: The characteristic oscillation induced by coupled processes between oceanic vertical modes and atmospheric modes in the tropical Pacific, *Geophys. Res. Lett.*, **28**, 2847-2850.

Yeh S.-W., and B. P. Kirtman, 2004: Tropical Pacific decadal variability and ENSO amplitude modulation in a CGCM. *J. Geophy. Res.*, **109**, C11009, doi:10.1029/2004JC002442.

Yeh, S.-W., J.-S. Kug, B. Dewitte, M. Kwon, B. P. Kirtman, and F.-F. Jin, 2009: El

Niño in a changing climate. *Nature*, **461**(7263), 511-514, doi:10.1038/nature08316.

Zebiak, S. E. and M. A. Cane, 1987: A model El Niño Southern Oscillation. *Mon. Wea. Rev*., **115**, 2262-2278.

Zhang, R.-H., and S. Levitus, 1997: Structure and cycle of decadal variability of upper ocean temperature in the North Pacific, *J. Climate*, **10**, 710-727.

국문 초록

엘니뇨 남방진동(ENSO)은 적도 태평양의 바람응력과 해양 열용량의 재충전/방출과 관련이 있다. 본 논문은 서태평양 지역 표층 바람 응력과 해양 성층화 특성과, ENSO 십년 주기 변동에 대한 바람과 해양 성층화의 역할을 조사하였다. 이와 같은 특성을 이해하기 위하여 연직 경압모드에 대한 표층 운동량의 기여도가 주로 논의되었다; 1) 바람응력과 해양 성층화의 관계, 2) 연직 경압모드-ENSO의 관련성 변화, 3) 최근의 온난역 해수면온도의 변화와 이것의 해양 성층화와 연관성. 해양에 바람응력이 미치는 효과를 찾기 위해 해양 성층화와 관련된 연직 경압모드가 조사되었고, 이것은 부력진동수로 이루어진 Sturm-Liouville 방정식의 해로부터 유도된다. 1958-2004년 동안의 SODA 자료 (바람응력, 해양온도, 염분, 해류)와 Hadley 해수면 온도 자료가 이용되었다. 또한, 물리적인 메커니즘을 자세히 이해하기 위해 간단한 접합 모델이 구성되었다.

관측에서, 서태평양 지역 바람 응력 컬이 1970년대 후반 이전보다 1970년대 후반 이후에 약해졌고, 이것은 적도에서 열용량의 느린 방출과 관련이 있다. 약해진 바람 응력 컬은 ENSO의 주기를 길게 하고 강도를 강하게 한다. 간단한 접합 모델 실험을 이용하여 서태평양 지역 바람 응력이 ENSO 절정기에 해양에 강하게 투영될 때 ENSO의 주기와 진폭이 감소하는 것을 확인하였다.

해양 경압모드에 대한 바람 투영 계수는 십년 주기 변동에서 유의한 변화를 보이고 첫 번째 모드와 두 번째 모드는 1970년대 후반 전후로 관련성이 상반되는 변화를 보인다. 1970년대 후반 이전과 비교해서, 첫 번째 모드는 적

도 파동 역학 때문에 해수면 온도에 더 큰 영향을 미친다. 또한, 대기 강제력에 대한 두 번째 경압모드의 변동성의 지연반응이 1970년대 후반 이후에 증가한다는 것이 발견되었다. 이것은 기후 변동과 관련한 ENSO 되먹임 과정의 변화를 반영한다.

바람 응력의 변화가 작게 나타나는 서태평양 온난역의 평균 해수면 온도가 증가하였다. 증가된 해수면 온도는 상층의 연직 성층화를 강화시킨다. 온난역의 해수면 온도 변동성은, 온난역의 첫 번째 경압모드에 투영되는 바람 응력에 의해 얻어진 최대 부력 진동수의 변화와 높은 상관성이 있다. 1970년대 후반 이전에, 첫 번째 경압모드에 대한 바람 응력의 회귀 분포는 동태평양과 중태평양 지역의 해수면 온도 편차와 관련이 있다. 반면 1970년대 후반 이후에, 첫 번째 경압모드에 대한 바람 응력 회귀분석 분포는 온난역의 동쪽 경계 근처에서, 바람의 수렴 패턴이 뚜렷하다. 온난역 지역의 해양 성층화 변화는, 해양 경압모드에 투영되는 바람응력의 변화와 관련이 있고, 이것은 최근에 관측된 엘니뇨 구조의 변화에 기여할 수 있다.

주요어: 엔소, 연직 경압모드, 바람응력, 해양 성층화, 십년 변동, 온난역
학번: 2004-30945